Hindawi
International Journal of Antennas and Propagation
Volume 2022, Article ID 1736377, 25 pages
https://doi.org/10.1155/2022/1736377

Research Article

Design and Study of a Miniaturized Millimeter Wave Array Antenna for Wireless Body Area Network

Abdullah G. Alharbi,[1] **H. M. Arifur Rahman**,[2] **Mohammad Monirujjaman Khan**,[2] **Muhammad Inam Abbasi**,[3] **Amani Abdulrahman Albraikan**,[4] **and Faris A. Almalki**[5]

[1]*Department of Electrical Engineering, Faculty of Engineering, Jouf University, Sakaka 42421, Saudi Arabia*
[2]*Department of Electrical and Computer Engineering, North South University, Bashundhara, Dhaka 1229, Bangladesh*
[3]*Centre for Telecommunication Research & Innovation (CETRI), Faculty of Electrical and Electronic Engineering Technology (FTKEE), Universiti Teknikal Malaysia Melaka (UTeM), Melaka 76100, Malaysia*
[4]*Department of Computer Science, College of Computer and Information Sciences, Princess Nourah bint Abdulrahman University, P. O. Box 84428, Riyadh 11671, Saudi Arabia*
[5]*Department of Computer Engineering, College of Computers and Information Technology, Taif University, P.O. Box 11099, Taif 21944, Saudi Arabia*

Correspondence should be addressed to Mohammad Monirujjaman Khan; monirujjaman.khan@northsouth.edu

Received 6 February 2022; Revised 26 March 2022; Accepted 29 March 2022; Published 9 May 2022

Academic Editor: Eng Hock Lim

A miniaturized millimeter wave (mmWave) antenna for wireless body area networks is proposed in this paper. The antenna is found to be operational in the V-band, around the 60 GHz frequency range, with high efficiency of up to 99.98% in free space simulations. A multilayer, thin substrate was implemented in the design to enhance radiation efficiency and gain. The antenna seems to be most suitable for small electronic devices and wireless body area network (WBAN) applications because of its low profile and lighter weight concept. To enhance its performance, several arrays of different orders were created. The Parallel-Fed and Tapered Feed Line methods were followed to design the planar arrays with 1×2, 1×4, and 2×2 elements in the primary design. Free space results were compared, and a 2×2 element array was found to be the most balanced according to the simulations. To justify the eligibility of these designs for WBAN applications, a virtual human body model was created within the 3D computer-simulated environment and the simulations were repeated, where four equal-spaced distances were taken into account to identify the antenna and its array behavior more accurately. Simulations returned optimistic results for the 2×2 element planar array arrangement in almost all parameters, even when placed close to the human body at any distance greater than 2 mm.

1. Introduction

The millimeter wave spectrum range is popular among antenna researchers for its high data transfer rate capabilities compared to shorter frequencies, although it covers a shorter distance before being absorbed by the atmospheric elements. More research has been conducted for further development of utilizing this spectrum when the 60 GHz standard is declared license-free, with a 7 GHz bandwidth (from 57 GHz to 64 GHz) by the Federal Communications Commission (FCC), where a gigabit per second data transfer speed can be achieved [1–3].

Since antennas play a vital role in any radio or wireless communication system [4–6], designing an efficient antenna with a better gain and a smaller size remains a challenge for researchers. In this context, microstrip patches or planar antennas are very popular in radar, mobile, and other wireless applications where compact size is one of the major

priorities. Their compact size, lightweight configuration, and simplified structures make them most suitable for ultra-wideband (UWB) or millimeter wave (mmWave) antennas. While achieving higher gain is also a challenge for small form factor (SFF) antennas like microstrip antennas, this issue can be solved by arranging antennas in arrays. There are different techniques for placing antenna elements in an array. A common classification, which divides the arrays into two types based on how they are arranged, is the series-fed array, while the other is the parallel-fed array antenna. Series-fed antennas are those antennas whose elements are connected in series with a single transmission line fed from the excitation. On the other hand, a parallel-fed antenna has multiple radiating elements connected by separate feeding lines. Different techniques have their own specific benefits. For example, parallel-fed antennas have a wider bandwidth than series-fed arrays, with 10% of the operating frequency compared to 1–3% of the operating frequency of series-fed ones [7]. A combination of these two is also available [8–10]. Whatever the technique is, the ultimate goal for making antenna arrays is to achieve one or more better antenna parameters.

Apart from other positive factors, microstrip antennas offer narrow bandwidth and lower gains. However, researchers investigated coupling methods to overcome these drawback issues by implementing antenna arrays. One of the prominent applications of these microstrip antennas is the wireless body area network (WBAN), where essential human physical data is collected with the help of placing several nodes on the body in various locations. These nodes gather this information and send it to the base station or the server with the help of a master node. WBAN or WBCN (Wireless Body-Centric Network) is mostly used for patient status monitoring in healthcare centers or monitoring an athlete's vital health signs in sports. To operate these tiny electronic devices wirelessly, embedded antennas must be lightweight, power-efficient, and small in size, making microstrip antennas the best candidate for the job. Manufacturing microstrip antennas is also budget-friendly, less complicated in structure, and much more convenient to integrate. The size of the antennas remains pretty small even when they are arranged in lower-order arrays, i.e., 2×2 or 4×1, etc. An antenna for a wireless body area network needs to be compact in size, printed, and flexible in design. The antenna also needs to have very good performance parameters to establish power-efficient communication links over the body-mounted wearable nodes. The antenna also needs to have a large bandwidth for high data rate communications. In a wireless body area network, the antenna also needs to have a high gain to allow communication with other colocated devices over the body surface of the human body. The major problem is that, due to the human body's lossy tissues, the performance of the antenna changes from the free space of operation. It is very important to check the performance of the antenna on the human body in order to check its suitability for the body area network. The antenna for WBAN applications also needs to be less sensitive to the human body.

Producing antenna arrays brings many advantages compared to a single-element antenna, such as increasing gain, creating wider bandwidth, neutralizing interference from a specific direction, increasing the signal-to-noise ratio (SNR), and precisely detecting the direction of the received signal. Several researchers proposed various series-fed array designs to increase their gain and bandwidth. [11–14]. At the joining point of the feed line and the patches, discontinuities in the junction cause phase shifts in the radiators. Moreover, the impedance matching technique becomes mandatory for the higher-order arrays. [15] To avoid this challenge, many researchers kept their arrays smaller. Besides this, smaller microstrip arrays mostly solve the gain and bandwidth issues that occur in a single-element antenna.

A novel Series-Fed Linear Microstrip antenna array with 23 identical antenna elements is proposed by Pratigya Mathur et al. [15] with a high gain of 19 dB. The antenna operates in Ka. A shorter version of this with 7 elements was fabricated and found to have a gain of 15 dB at 5.79 GHz. A 3×3 element array antenna was simulated by Vasujadevi Midasala et al. and found to have a gain enhancement, which recorded a maximum gain of 17.29 dB at 13.33 GHz. The antenna operates between 12 GHz and 18 GHz [16]. Bala B.D. et al. have investigated a 2.4 GHz antenna and analyzed and compared its performance by making it 1×2, 2×2, 1×4, and 2×4 arrays, where they were able to achieve 10.1 dB of gain with a radiation efficiency of 45% at 2.44 GHz. There is also a little research on array antennas that operate in the millimeter-wave spectrum. Young-Jun Kim et al. proposed a 2×2 array antenna with 12.5 dBi that was operational at 28 GHz [17]. An array of 4×4 antenna elements was proposed by M. Weiss, working at 36.6 GHz, 38.4 GHz, and 57.4 GHz with a maximum efficiency of 79%. [18] Hamsakutty Vettikalladi et al. stacked array antenna with a 30 mm × 30 mm dimension recorded a max gain of 18.07 dB [19] with 68.3% efficiency at 60 GHz, which was a 4×4 element design. In [20–22], authors have proposed different broadband antennas with good performance parameters, but the antennas work at lower frequency bands. The antennas were designed on Rogers RT/Duroid with a relative permittivity of 2.2. The antennas presented in [20–22] were not proposed for wireless body area networks. A textile-based wearable 60 GHz mmWave antenna for body-centric communication is proposed in [23]. First, the antenna was designed on a 100-polyester substrate, and then, it was designed on different other textile substrates. The antenna has an 11.63 GHz impedance bandwidth and shows a gain of 5.96 dBi. The antenna is a single element, and it has an overall length and width of 12.2×12 mm. A cotton-based mmWave array antenna for body-centric communications is presented in [24]. The antenna has an impedance bandwidth of 10 GHz and shows very low radiation efficiency. The overall size of the antenna proposed in [24] is larger.

In this paper, a design for a very small-sized mmWave antenna is presented with only a 3.96 mm long patch radiator, operating between 45 GHz and 62.5 GHz. Parallel-fed antenna arrays were designed with this element in several dimensions, such as 1×2, 1×4, and 2×2, and their simulated results were compared with each other. A human

body torso was created to check these array antennas' human performance on body performance. Several distances from the human body were also taken into account while comparing the simulated results. Though these results were computer simulation-based, simulations done in the CST environment were verified and found adequate through numerous research worldwide. Finally, a conclusion was drawn based on these results.

2. Antenna Design

The antenna was designed and tuned to operate in the 60 GHz range within the V-band of millimeter waves. A Microsoft Windows-based popular simulation software named "Computer Simulation Technique (CST) Microwave Studio Suite" was used to design the antenna and simulate it to check the desired parameters. The antenna, though having a similar look to the earlier design presented in [25], is actually a miniaturized version, which was done by reducing the size in all dimensions. It was a challenge to keep the design operational at the same desired frequencies while making it smaller and keeping the similar look. Therefore, further tuning and parametric studies were done, and many structural dimensions were changed. In particular, the substrate part was completely restructured. Figure 1 shows the antenna model from different perspectives.

The total antenna with the substrate is 5.12 mm long and 3.28 mm wide with a quasi-self-complementary design. At 60 GHz, the wavelength of the proposed antenna is 5 mm. The electrical size of the overall substrate length and width of this antenna is 0.97λ and 1.52λ, respectively. The antenna consists of multiple layers with a sandwiched air gap layer within the substrate. The material used as the substrate is Rogers RT5880, with a permittivity of 2.2 and a loss tangent of 0.001. The substrate, which is in total 0.306 mm thick, includes the 0.18 mm air gap layer between the 0.063 mm walls of RT5880 on both sides. This carefully equalized thickness of the air gap was introduced to increase the antenna gain. On the top of the substrate, the radiator patch is located, which is the main antenna element for the 60 GHz operating frequency. By varying the size of this top radiating element, the operating frequency and the impedance bandwidth can be changed for this antenna. The radiator part alone is only 3.96 mm long and 1.54 mm wide. The length and width of the radiating element have an electrical size of 1.26λ and 3.24λ, respectively. The patch part is made of Perfect Electric Conductor (PEC) material. The thickness is kept at 0.035 mm. Below the substrate, the lowest layer is the ground, with a thickness of 0.035 mm, the same thickness as the radiator. This ground plane at the backside of the antenna usually helps to reduce the effects on human body tissues. Annealed copper was used for the ground with a conductivity of 5.8×107 S/m. Including all the layers with the air gap, the total thickness of the antenna is 0.376 mm.

The radiator patch has a feed of 2.01 mm long and 0.53 mm wide, connecting the waveguide port on the bottom and the main radiator patch. The patch is a combination of a half-elliptical part at the bottom and a half-triangular part at the top, with a 0.041 mm wide isosceles triangular slot in the middle. The slot is introduced to the top radiating element for impedance matching and wide bandwidth purposes. The equal sides of the triangle are 1.37 mm long, and the base is 1.23 mm. A 0.82 mm long and 0.37 mm wide rectangular brick is placed in the middle to tune the resonant frequency, with a pair of 0.082 mm slots on top and below it. The tip of the triangular part is sawed to make a 0.34 mm horizontal edge. The detailed dimensions of the radiator patch are shown in Figure 2(a). On the other side of the substrate, the ground design is combined with a circular, triangular, and rectangular cutout. This helps to achieve a larger bandwidth of the antenna. The center of the circle slot is horizontally aligned in the middle of the substrate but vertically slightly shifted upward. The triangular slot was extruded and joined with the circular slot. The existing arms are defined in Figure 2(b) by 1.29 mm and 1.66 mm.

In Figure 2(c), the thickness of the different layers of the antenna is given from a side view, where the rightmost layer is the ground and the leftmost is the radiator patch. The air gap between the substrate and the air gap, which is 0.18 mm thick, is represented by the wider layer in the middle.

Table 1 shows the different layers of the antenna with their corresponding thicknesses, materials used, and their relative permittivity.

3. Free Space Simulations

3.1. Return Loss. In Figure 3, displayed above, the return loss (RL) curve of the antenna is presented. It shows the operating zone of the antenna around the 60 GHz frequency range, with a bandwidth of 17.8 GHz. Though the resonant frequency is slightly below 60 GHz, it has quite comfortably achieved an RL value below-24 dB at the desired frequency and has the upper cut-off at 65.562 GHz.

3.2. VSWR. The curve below in Figure 4 shows the voltage standing wave ratio (VSWR) of the antenna. At 60 GHz, the VSWR value was 1.128, which is very close to unity.

The voltage standing wave ratio graph shown in Figure 4 displays a consistent curve related to the return loss curve of the antenna.

3.3. 3D Radiation Patterns. In Figure 5, a 3D radiation pattern at 60 GHz is presented for the designed antenna, which shows a maximum gain of 4.01 dB in the direction along the XY plane, inclined to the X-axis. The 3D radiation pattern of this antenna looks very close to the omnidirectional pattern. A slight distortion is noticed in the radiation pattern, which is for the antenna structure and very high operating frequency.

3.4. 2D Radiation Patterns. In Figure 6, the radiation patterns of the antenna from a two-dimensional view are presented for the XY plane and YZ planes at 60 GHz frequency in Figures 6(a) and 6(b), respectively. Patterns are similarly omnidirectional on both planes.

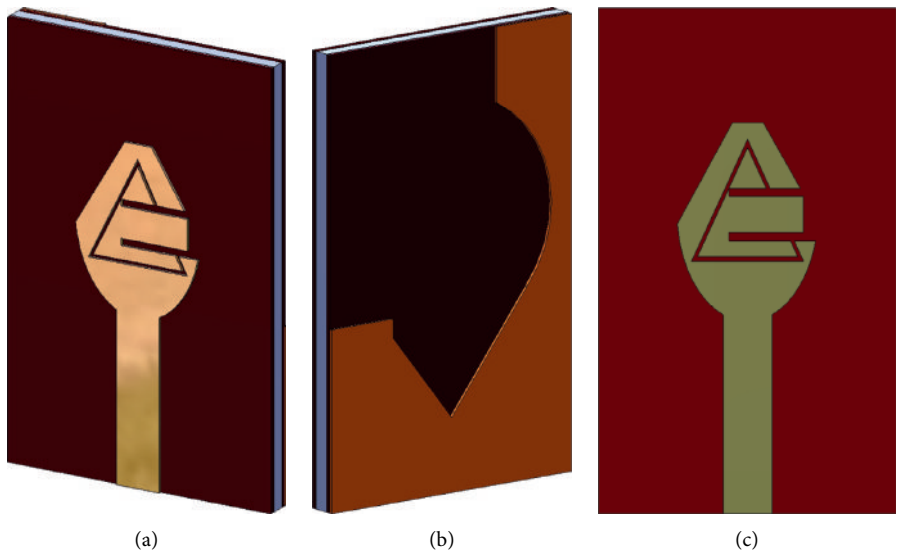

Figure 1: Miniaturized antenna model in different views: (a) 3D front, (b) 3D back, and (c) front.

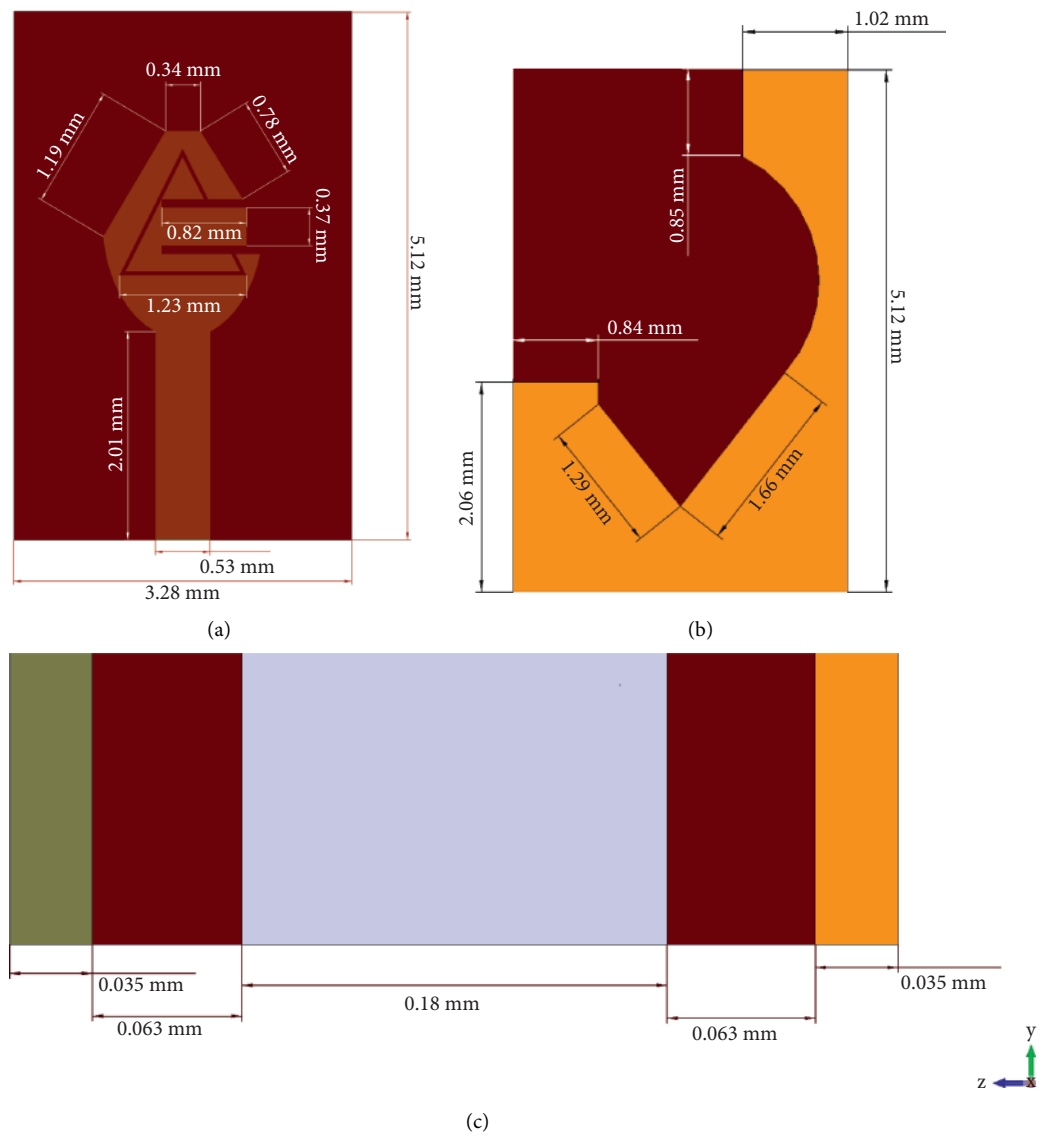

Figure 2: Antenna dimensions (a) front dimensions, (b) back dimensions, and (c) layer dimensions.

Table 1: Antenna materials.

Parameter	Thickness (mm)	Material	Epsilon
Ground	0.035	Copper (annealed)	—
Substrate	0.306 (with gap)	Rogers RT5880	2.2
Air gap	0.18	Air	1.00059
Patch radiator	0.035	PEC	—

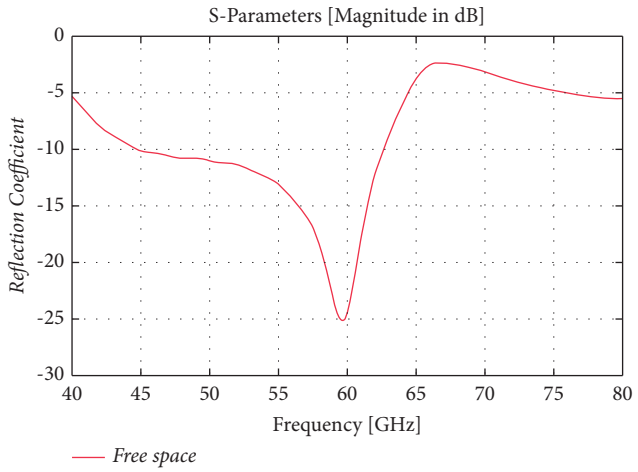

Figure 3: Return loss of the antenna in free space.

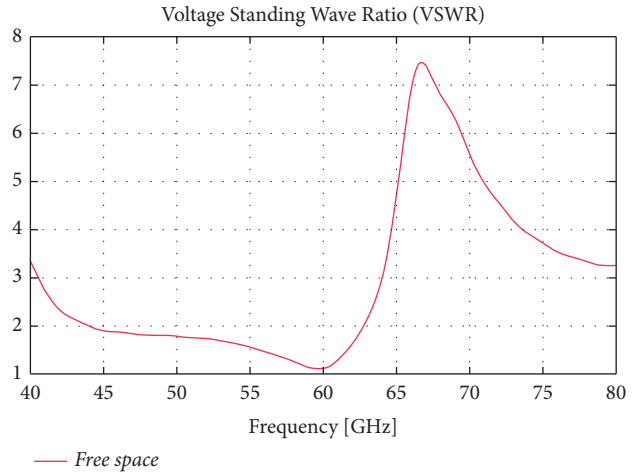

Figure 4: VSWR for free space.

3.5. Surface Current. Surface current distribution on the ground and radiator patch is presented in Figure 7 when the antenna is excited from the connected waveguide port 1. Maximum current distribution is noticed over the top radiating element and near the feed of the antenna. Here, Table 2 shows the other parameters of the antenna. The antenna, having a bandwidth of 17.8 GHz, achieved a maximum gain of 4.01 dB with a radiation efficiency of 99.98%.

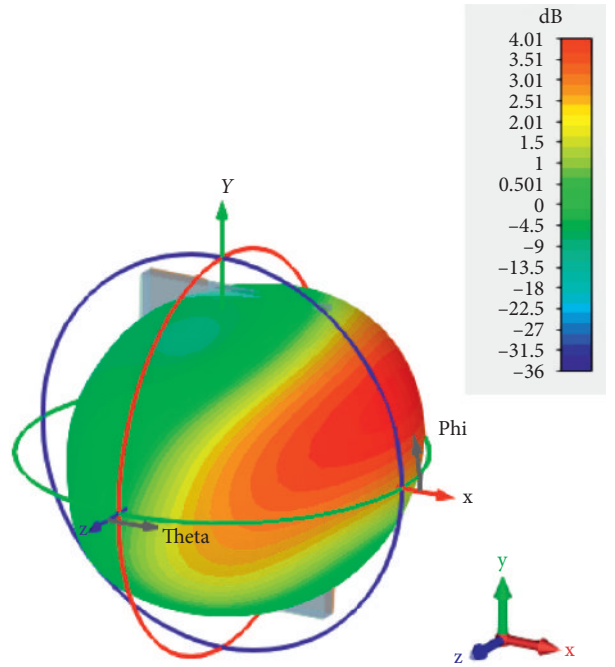

Figure 5: 3D radiation pattern in free space for at60 GHz.

4. Array Design

4.1. 1 × 2 Array Design. In order to improve the performance, this antenna was designed again as an array structure. A 1 × 2 array was designed with the earlier presented antenna with tapered lines and a parallel feeding technique (as shown in Figure 8). The substrate is 10.49 mm long horizontally and 7.17 mm vertically. Tapered feeds were made half the width gradually from the element's feeds, each with a 100-ohm $\lambda/4$ line to divide the power equally and connected to the 50-ohm feed with the width of fw. The antenna elements were kept a λ_g distance apart; the technique followed from the [26] to enhance radiating gains, where λ_g is the guided wavelength:

$$\lambda_g = \frac{\lambda_f}{\sqrt{1 - \lambda_f/\lambda_c}}, \tag{1}$$

where λ_f/λ_c is the ratio between the wavelength in free space and the cutoff wavelength.

Or, simplifying more,

$$\lambda_g = \frac{\lambda_f}{\sqrt{1 - f_c/f}}, \tag{2}$$

where λ_f is the wavelength of the EM wave at free space, and f_c and f are the cutoff and operating frequencies, respectively.

For a substrate with a dielectric constant of εr,

$$\lambda_g = \frac{\lambda}{\sqrt{\varepsilon_r (1 - f_c/f)}}. \tag{3}$$

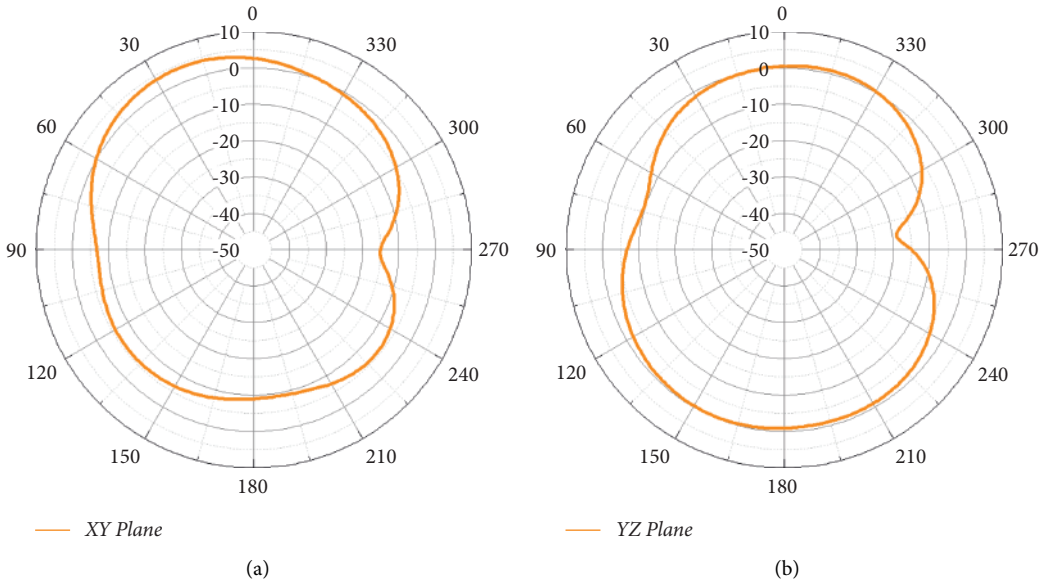

(a) (b)

Figure 6: 2D radiation pattern in free space at 60 GHz from (a) XY plane and (b) YZ plane.

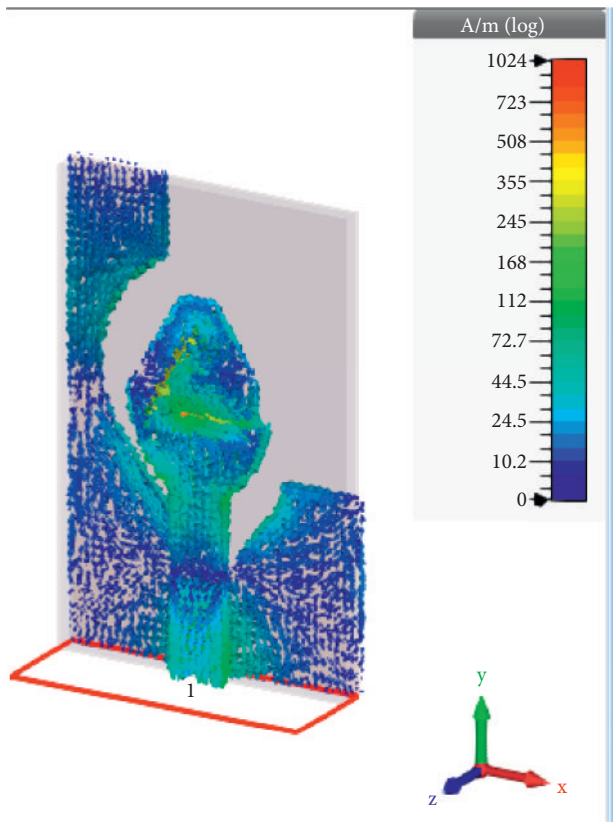

Figure 7: Surface current in free space at 60 GHz.

Table 2: Other antenna parameters.

Bandwidth (GHz)	Gain (dB)	Radiation efficiency (%)	Total efficiency (%)	VSWR
17.8	4.01	99.98	99.62	1.1283

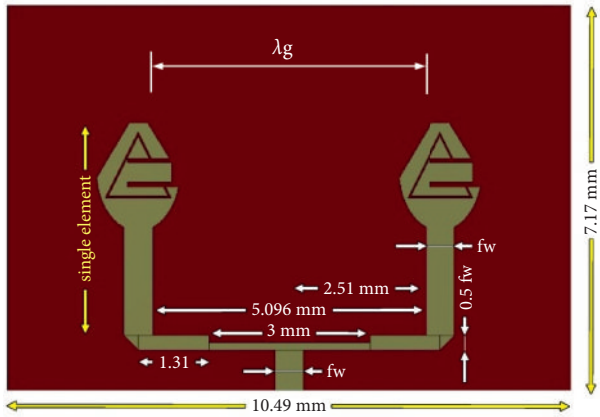

Figure 8: : 1 × 2 Array with the antenna.

Figure 9 shows the backside of the array where the element grounds were aligned according to the radiator patches on the front. As the waveguide port was on the bottom of the antenna, the grounds were connected to the port with a 1.00 × 1.02 mm rectangular connecter made with PEC. The connector is the same height as the ground. The same number of free spaces was kept outside the elements on both the ground and patches.

Figure 10 shows the 3D perspective views of the antenna. On the left, the two-element parallel-fed array antenna's front view is shown, while the back view is presented in the right figure.

The simulation results for the 1 × 2 design are given below.

4.1.1. Return Loss. The return loss response of the 1 × 2 array is shown above in Figure 11. The curve shows a wide bandwidth with an RL value of around 18.5 dB at 60 GHz.

4.1.2. VSWR. Figure 12 shows the VSWR curve of the 1 × 2 antenna array. The voltage standing wave ratio (VSWR) was found to be 1.27 at the desired frequency within the mmWave spectrum range.

4.1.3. Surface Current. In Figure 13, the surface current distribution is shown when the antenna is excited with the waveguide port 1. The maximum surface current recorded was 409 A/m in the radiator patch area.

4.1.4. 3D Radiation Pattern. The 3D radiation pattern of the 1 × 2 antenna is displayed in Figure 14, where the maximum gain was recorded in the main lobe's direction. The recorded maximum gain was 5.01 dB along the YZ plane. The 3D radiation pattern for the 1 × 2 array for the antenna looks distorted, which is due to the effect of the array element.

4.1.5. 2D Radiation Patterns. Figure 15 shows the two-dimensional radiation patterns of the antenna on both the XY and YZ planes. In Figure 15(a), the radiation pattern is shown on the XY plane where the sidelobe levels (SLLs) are lower than the main lobe. The main lobe magnitude was recorded at 2.42 dB with an angular width of 71.1 dB and the sidelobe level was −1.7 dB. The YZ plane exhibits an omnidirectional pattern. This 1 × 2 array structure shows improved gain compared to the single-element antenna.

4.2. 1 × 4 Array Design. Figure 16 shows the 1 × 4 element array design with the proposed antenna. This was designed with the view of improving the performance of the antenna further. Elements were separated with λ_g distance, as shown in Figure 17(a). Thick feeds connecting the middle elements are 2.63 mm long. Elements were connected horizontally. This parallel-fed design is connected with the same width 50-ohm feed line as the original element, with a waveguide port on the bottom.

On the other hand, grounds were parallel connected to the port with similar rectangular PEC connectors as the 1 × 2 array, as shown in Figure 17(b). The ground elements were aligned with the radiator patches on the front. Grounds were placed vertically in the middle of the substrate, keeping 1.024 mm gaps on top and bottom. Other detailed measurements are given in Figure 17.

The simulated parameters of the 1 × 2 array are given in the following sections.

4.2.1. Return Loss. The return loss response of the 1 × 4 array is presented in Figure 18. The RL value at the desired frequency is slightly higher than the value found on the 1 × 2 array but still under -16 dB. It seems there are no major benefits added to the RL curve by making it a 1 × 4 in terms of bandwidth and the return loss value.

4.2.2. VSWR. Figure 19 shows the VSWR curve of the 1 × 2 antenna array. The voltage standing wave ratio (VSWR) was recorded as 1.3295 at 60 GHz. The VSWR curve similarly responded to the frequency responses found in the return loss for the 1 × 4 array.

4.2.3. Surface Current. The surface current distribution of the 1 × 4 array is given in Figure 20 when the antenna is excited with the waveguide port 1. The maximum surface current recorded was 304 A/m near the rectangular brick in the radiator patch area.

4.2.4. 3D Radiation Pattern. In Figure 21, the 3D radiation pattern of the 1 × 4 antenna is shown where the maximum gain was recorded in the main lobe's direction along the YZ plane. The maximum gain recorded was 5.31 dB. Therefore, the major difference was found to be in the radiation pattern in terms of gain and better directivity. The 3D radiation pattern of the 1 × 4 antenna looks like a better shape than the 1 × 2 antenna array structure.

4.2.5. 2D Radiation Patterns. Figure 22 presents the 2D radiation patterns of the antenna on the XY (in Figure (a)) and YZ (in Figure (b)). In the XY plane's pattern, the

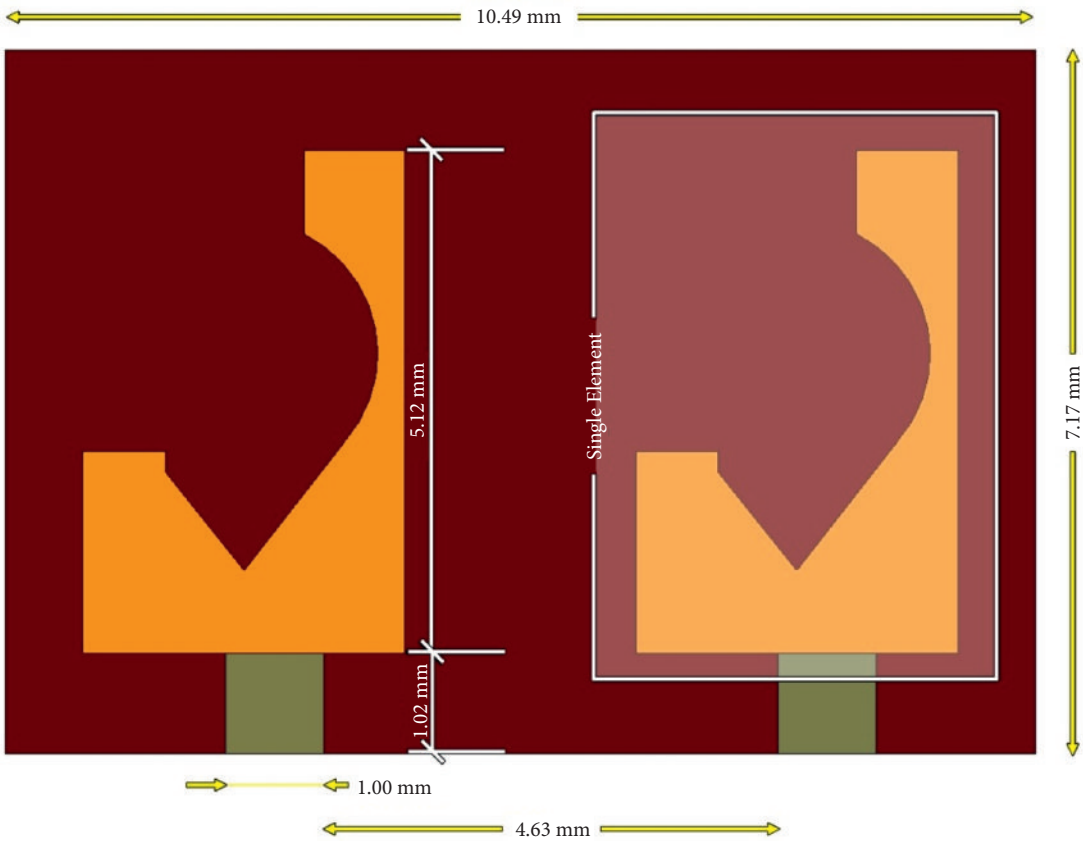

Figure 9: Back of the 1 × 2 array with the antenna.

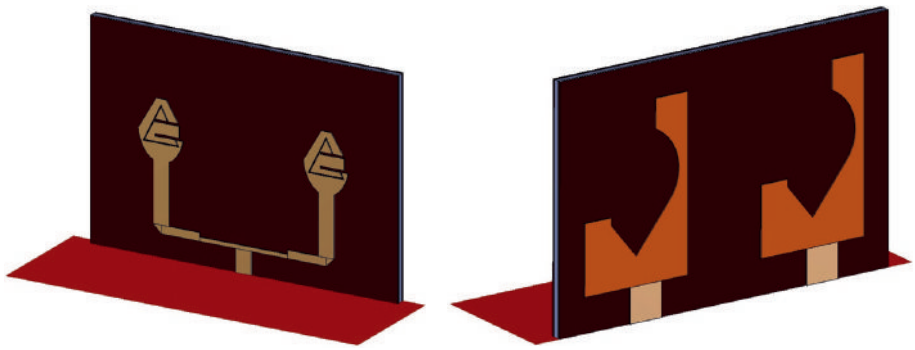

Figure 10: 3D view of the 1 × 2 antenna array.

sidelobe levels (SLLs) are lower than the main lobe, as in the previous array. The main lobe magnitude was recorded at 2.41 dB at 22° with an angular width of 60.3 dB, and the sidelobe level was -1 dB. The main lobe magnitude on the YZ plane was recorded at around 5 dB in a direction of 53°.

4.3. 2 × 2 Array Design. Another four-element array was designed with the antenna in a square matrix arrangement (2 × 2 array) to check the efficiency of the four-element array performance with different arrangements. The array was also constructed in a parallel-fed design. Figure 23 shows the 3D view of the 2 × 2 array with the antenna. Here, two 1 × 2 elements were connected with a 100 thin feed line. Thin transmission line feed width can be calculated using

$$w_f = \left(\frac{377}{z_0\sqrt{\varepsilon_r}} - 2\right) \times h. \quad (4)$$

The simulation results for the 2 × 2 antenna array are given below.

Figure 24 shows the dimensions of the different parts of the antenna. The total antenna array dimension in the front shown in Figure 24(a) is 10.486 mm × 14.366 mm. Vertically, two elements were kept 2.942 mm apart. The vertical thin feed is 6.4 mm long and connects the upper two elements with the main 50 feed.

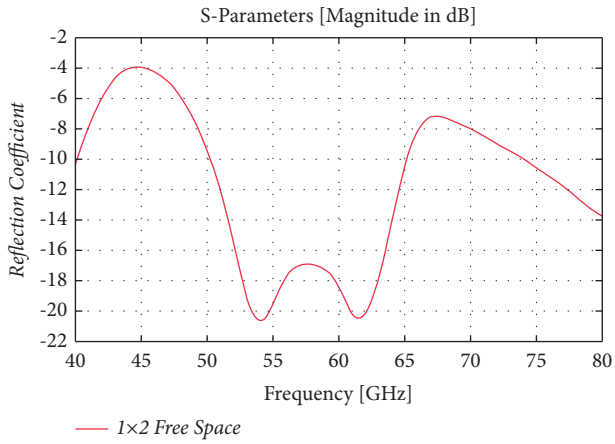

Figure 11: Return loss of the 1 × 2 antenna array.

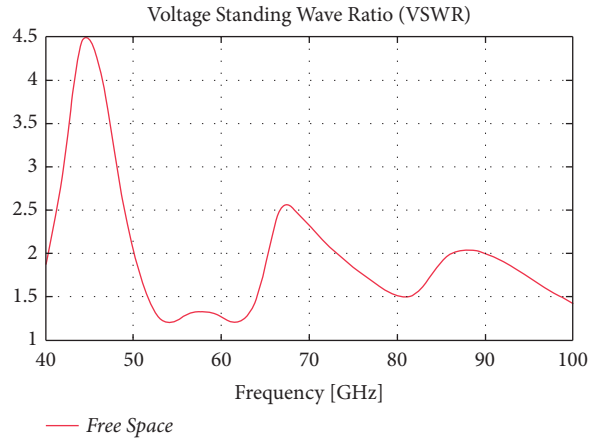

Figure 12: VSWR curve of the 1 × 2 antenna array.

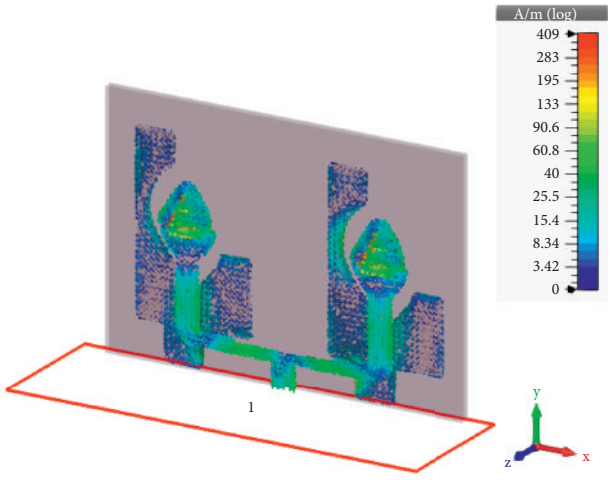

Figure 13: Surface current at 60 GHz of the 1 × 2 array.

4.3.1. Return Loss. Figure 25 shows the return loss response of the 2 × 2 antenna array. The return loss (RL) curve for the 2 × 2 antenna array shows a better result than the previous combinations shown earlier. At 60 GHz, the RL value was found to be below -15 dB, but the bandwidth is much wider.

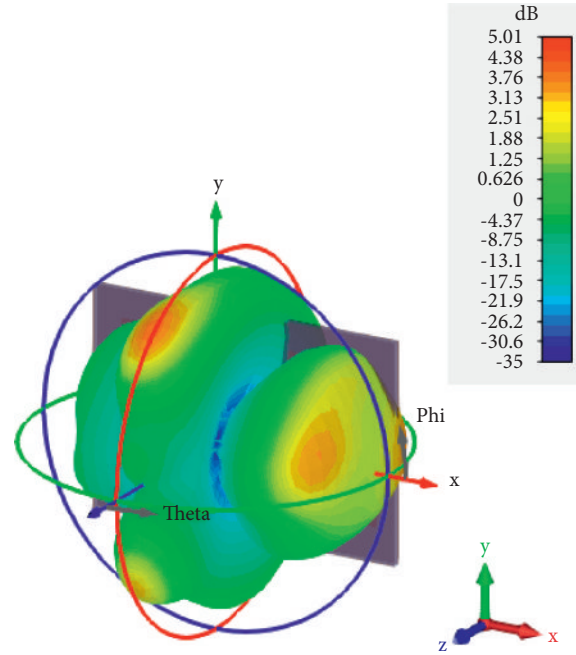

Figure 14: 3D Radiation pattern (1 × 2 array).

4.3.2. VSWR. Figure 26 shows the VSWR curve of the 2 × 2 antenna array. The maximum surface current was recorded at 346 A/m around the rectangular shape in the middle of the patch antenna elements. Figure 26 visualizes the surface current distribution of the 2 × 2 arrangement of the antenna array.

4.3.3. Surface Current. The maximum surface current was recorded at 346 A/m around the rectangular shape in the middle of the patch antenna elements. Figure 27 visualizes the surface current distribution of the 2 × 2 arrangement of the antenna array.

4.3.4. 3D Radiation Pattern. The 3D radiation pattern of the 2 × 2 array design is shown in Figure 28, where the maximum gain was recorded at 6.65 dB, which is a better increment than the other two array arrangements.

4.3.5. 2D Radiation Patterns. Figure 29 shows the 2D radiation patterns of the 2 × 2 antenna array arrangements. On the XY plane, in Figure 29(a), the radiation pattern exhibits around 6 dB of gain in the direction of 30° The angular width of the main lobe is 14.1° and the sidelobe level is -0.5 dB. This antenna shows the highest gain for the 2 × 2 array design structure.

4.4. Comparison. After simulating different antenna parameters for different array arrangements, the results are compared in the above figures. In Figure 30, return losses were compared for all three array designs with the single-element antenna. In terms of RL values, all the designs show satisfactory return loss values at 60 GHz frequency. Bandwidth has significantly increased for the 2 × 2 antenna array.

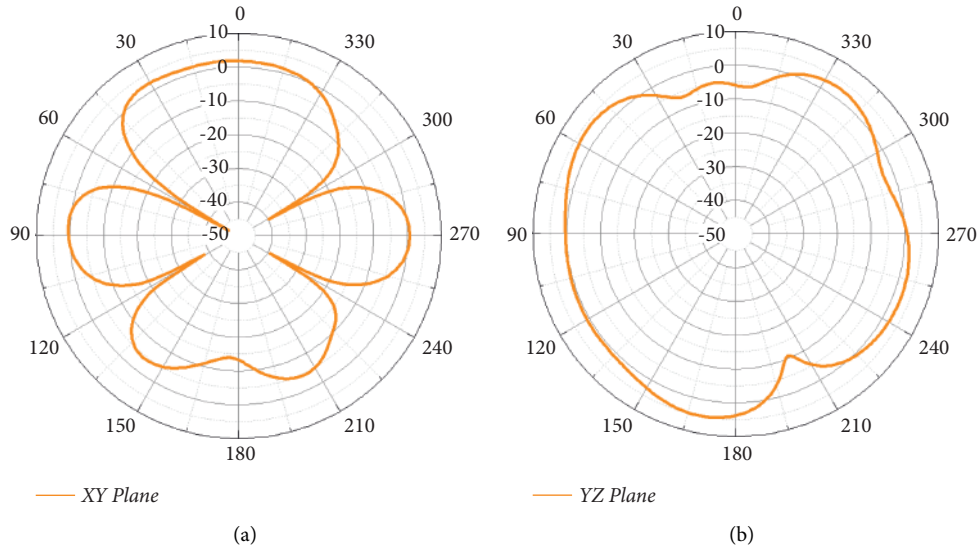

(a) (b)

Figure 15: 2D Radiation Patterns (1 × 2 Array) on (a) XY plane, and (b) YZ plane.

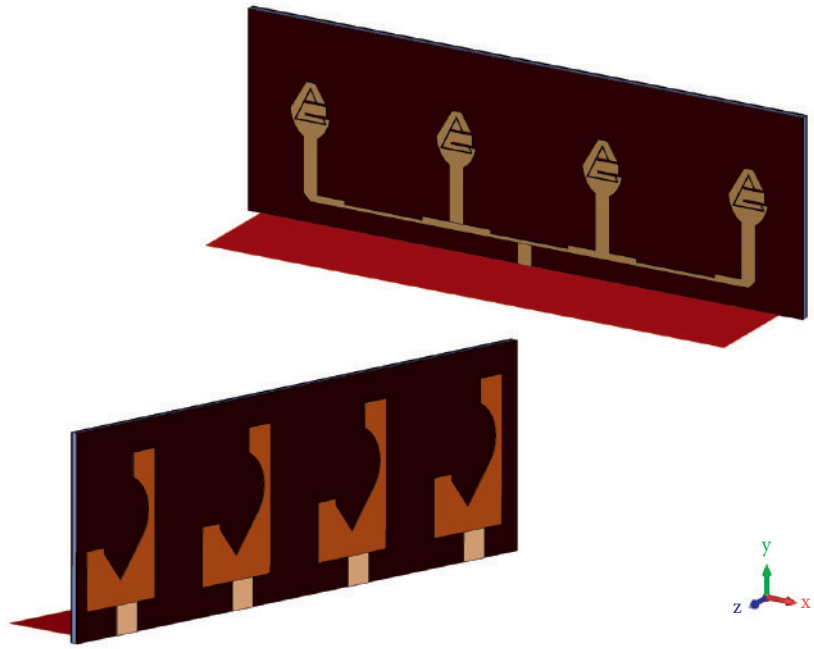

Figure 16: 1 × 4 array design.

In the next comparison shown in Figure 31, gains gradually increased for 1 × 1, 1 × 2, 1 × 4, and 2 × 2 arrangements, which is visible in Table 3. The radiation efficiency of the 2 × 2 was found to be more optimistic compared to other arrangements.

Therefore, the 2 × 2 antenna array shows the most promising results through the simulations.

In Table 3, radiation and total efficiency are significantly better than any other array arrangement. Radiation efficiency was 80.39% for the 2 × 2 array. Similarly, the bandwidth and gain for the array are also much higher than the others. The gain of the array was 6.65 dB, while the single element was 4.01 dB. In terms of parameter improvement, the 2 × 2 array buildup was a successful attempt.

5. On-Body Performance Test

To check the eligibility of the antenna in the wireless body area network (WBAN), it is necessary to check the effectiveness of the antenna in close proximity to a human body. Though the penetration depth of human skin by a 60 GHz millimeter wave is just a half millimeter [27], the presence of the human body greatly affects the antenna parameters like bandwidth, efficiency, return loss value, gain, and radiation patterns. Due to the capacitive nature of the human body, these parameters fluctuate [26].

For this reason, a three-dimensional human body model was made, consisting of the three outermost layers of the human body: skin, fat, and muscle (see Figure 32). The

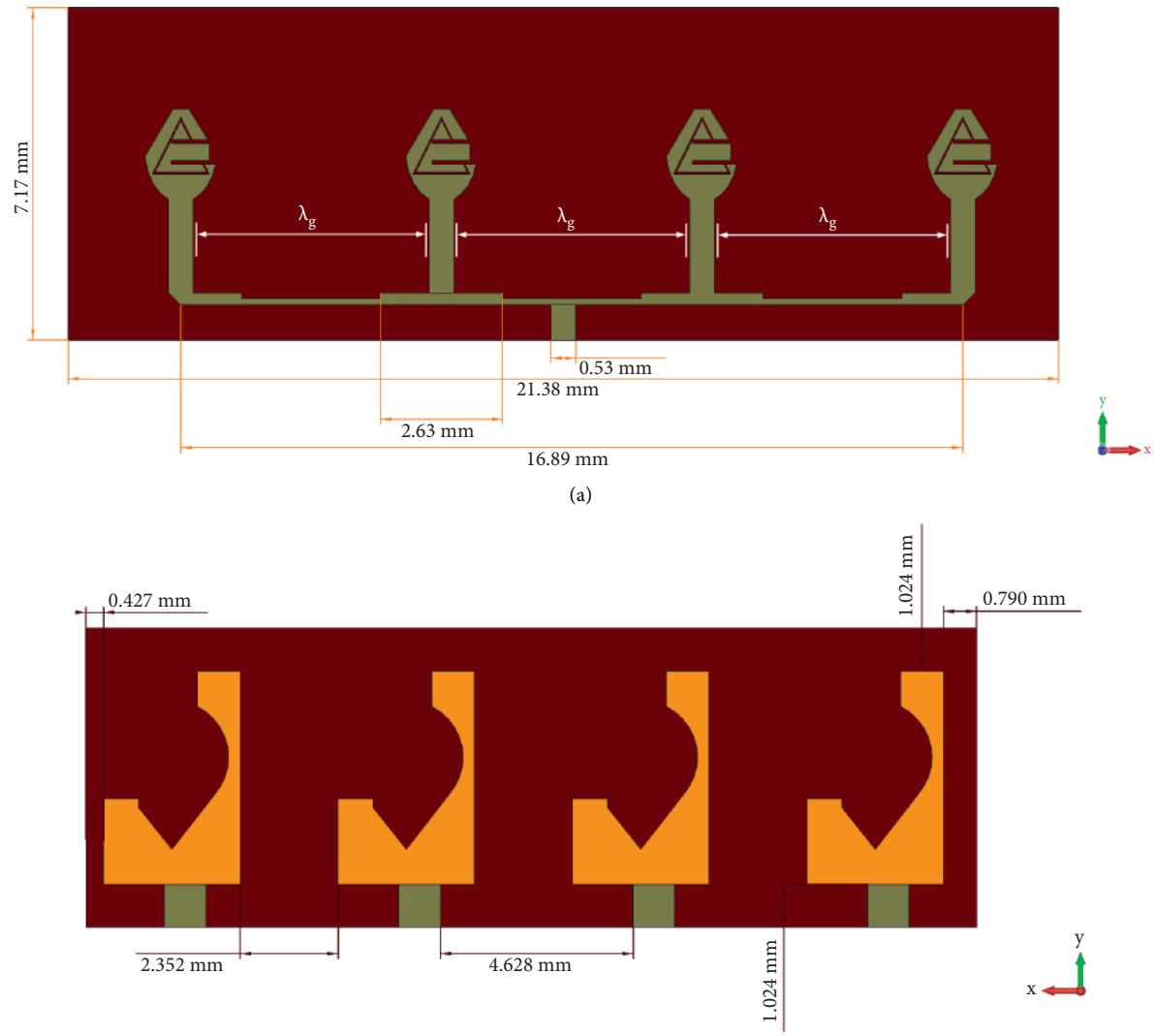

Figure 17: Design parameters.

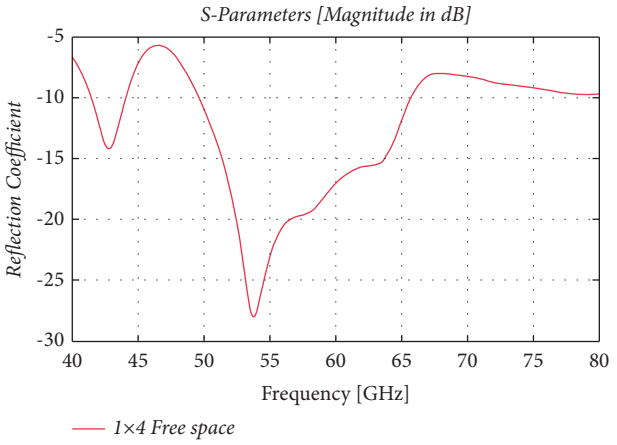

Figure 18: Return Loss of the 1 × 4 antenna array.

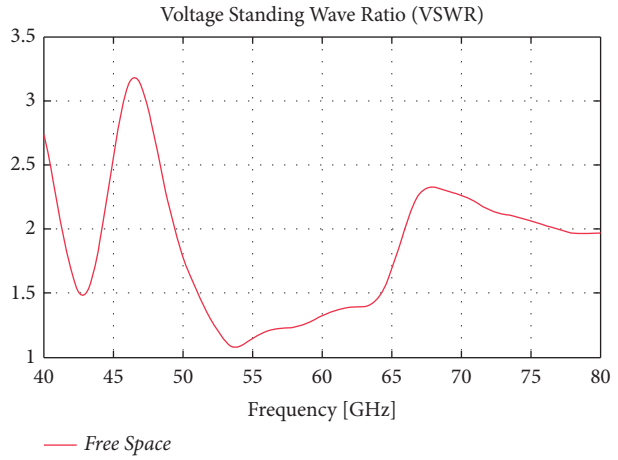

Figure 19: VSWR curve of the 1 × 2 antenna array.

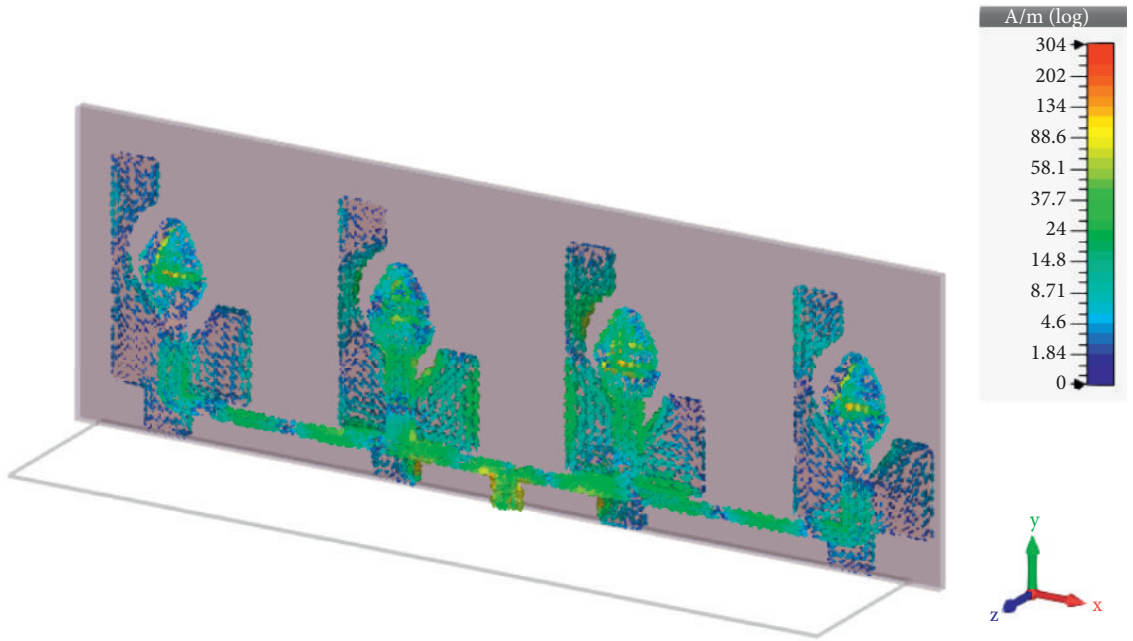

Figure 20: Surface current at 60 GHz of the 1 × 2 array.

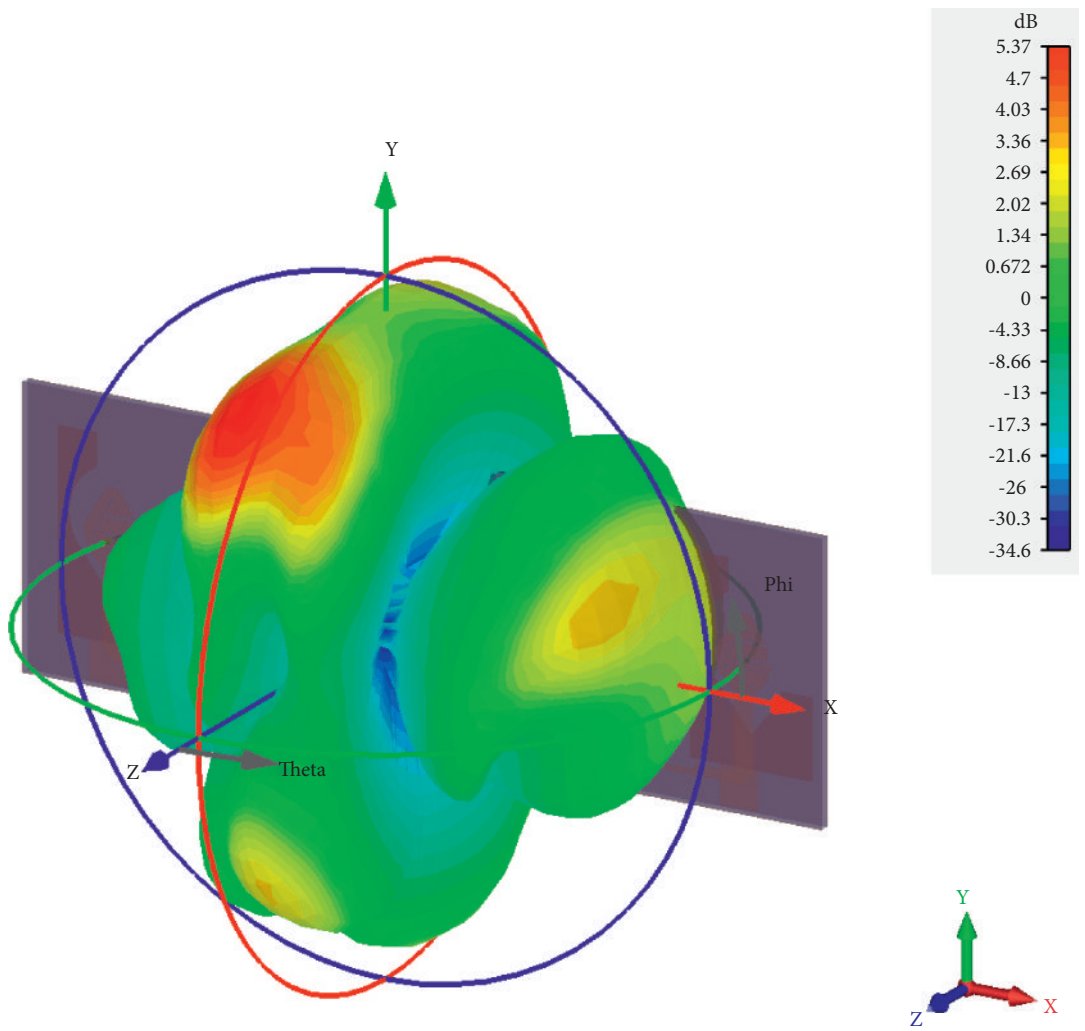

Figure 21: 3D Radiation pattern (1 × 4 array).

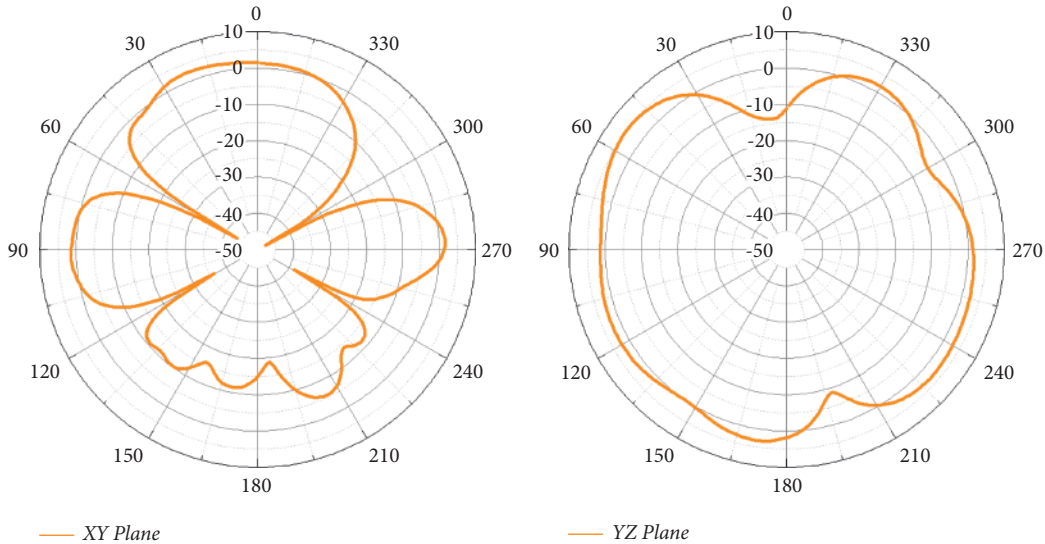

Figure 22: 2D radiation patterns (1 × 4 array) on (a) XY plane and (b) YZ plane.

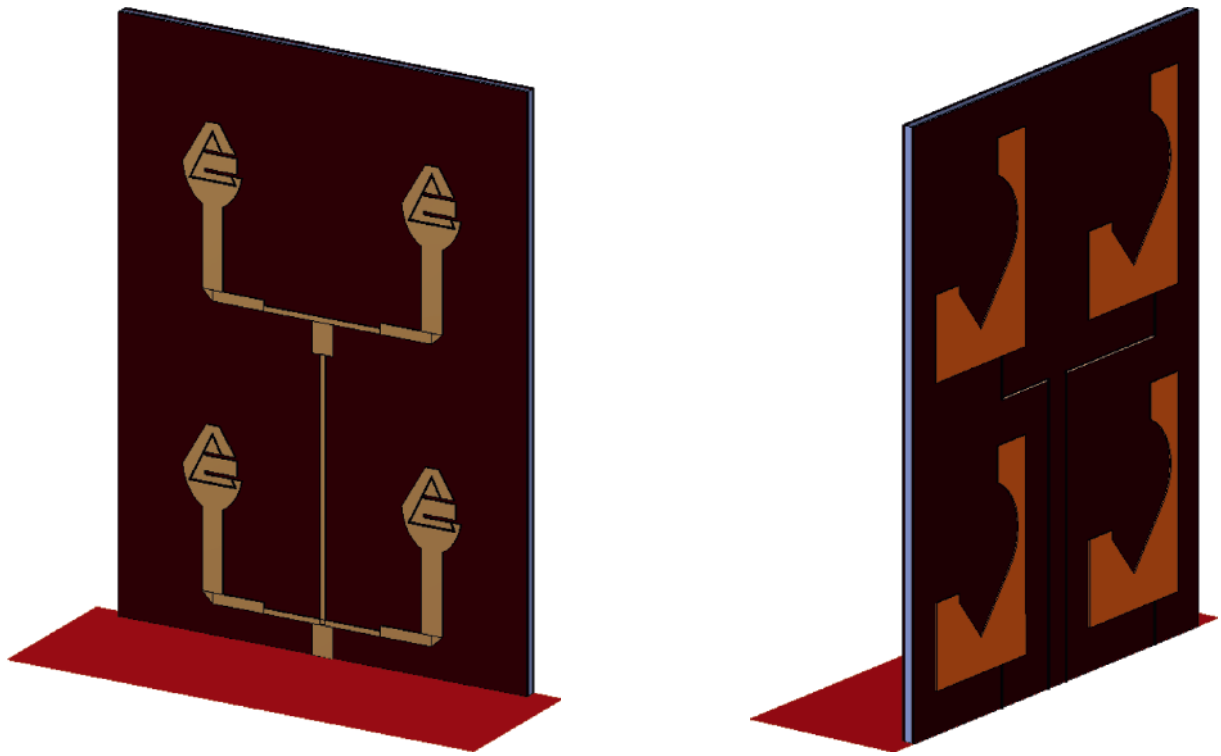

Figure 23: 3D view 2 × 2 array with the antenna.

model was built using the CST Microwave Studio Suite, including all the necessary electromagnetic properties of these body layers. First, a 1.3 mm thick skin layer was created with its specs, i.e., permittivity, conductivity, concentrations, etc. [28]. Similarly, a fat layer was created with a thickness of 3 mm adjacent to it. The innermost of these, the muscle layer, was also created and attached to it sequentially. For simulation purposes, 3 mm of the depth of the muscle layer was taken. The whole model is 7.3 mm thick. To achieve a more accurate result, the created human body model's length and width were kept greater than the value of 4.

The created multiple array designs were then tested on the human body model by placing the antenna in four gradually increasing equidistant places, as shown in Figure 33, and resimulating all the parameters. Finally, the results are compared and commented upon the simulated results.

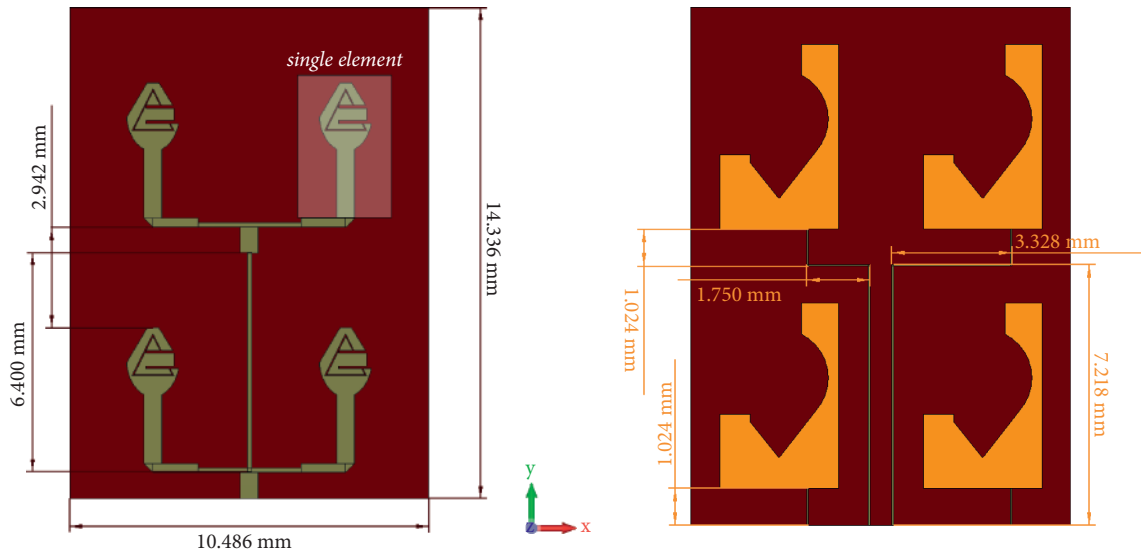

(a) (b)

Figure 24: Back dimensions of the 2 × 2 array.

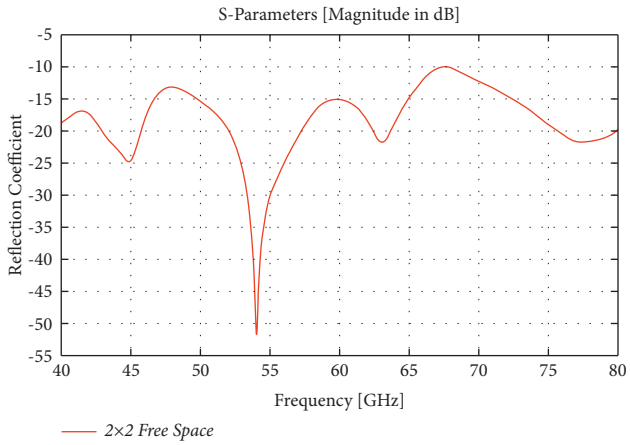

Figure 25: Return loss of the 2 × 2 antenna array.

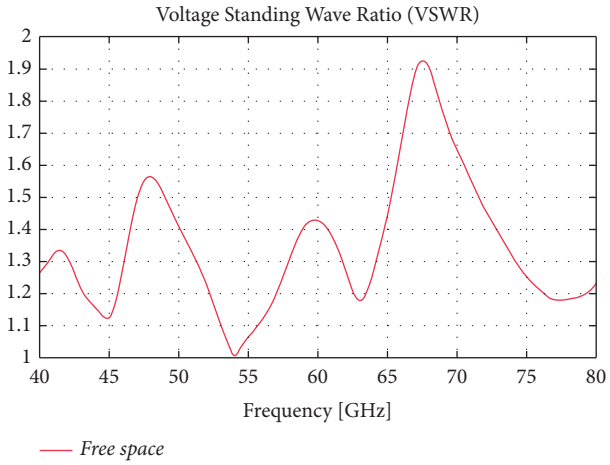

Figure 26: VSWR curve of the 2 × 2 antenna array.

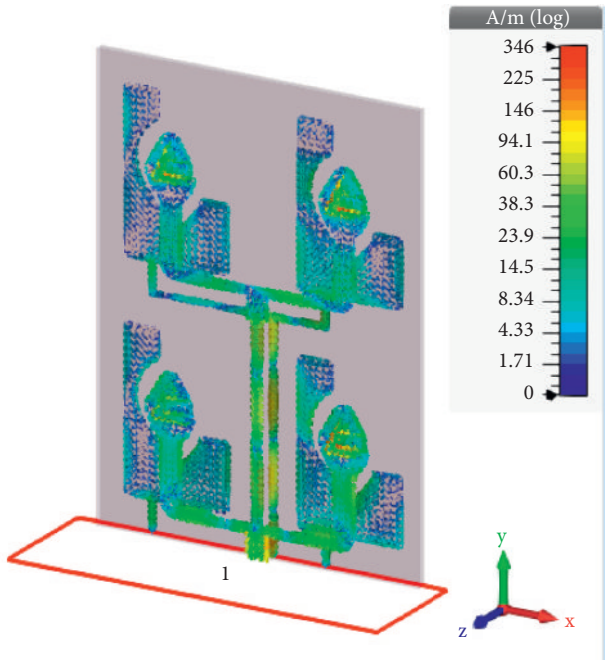

Figure 27: Surface current at 60 GHz of the 1 × 2 array.

For the single element, 1 × 2 and 2 × 2, the dimensions were kept the same as for the model, which was 16 mm × 19 mm (given in Figure 34(a)). To ensure radiation coverage for the 1 × 4 array's elongated horizontal structure, the dimension was modified to 28 mm × 19 mm (Figure 34(b)).

During the distance-based study, the antennas with different array arrangements were placed at four equal gap distances, starting from 2 mm to 8 mm, for each array, and the results were simulated to check and compare with each

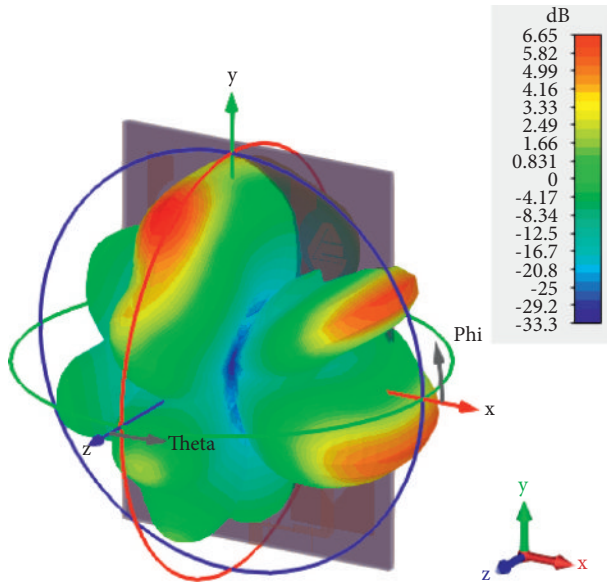

Figure 28: 3D radiation pattern (2 × 2 array).

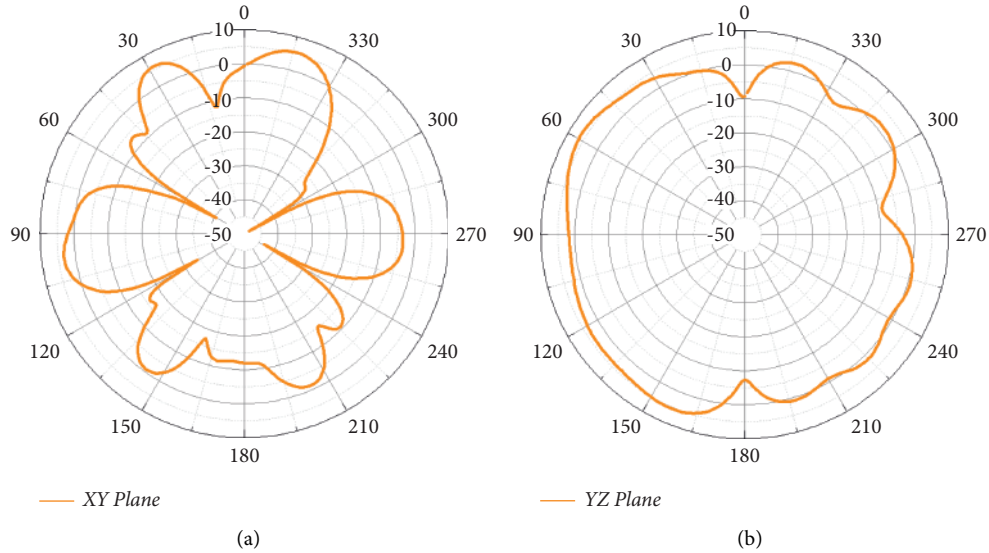

(a) (b)

Figure 29: 2D radiation patterns (2 × 2 Array) on (a) XY plane and (b) YZ plane.

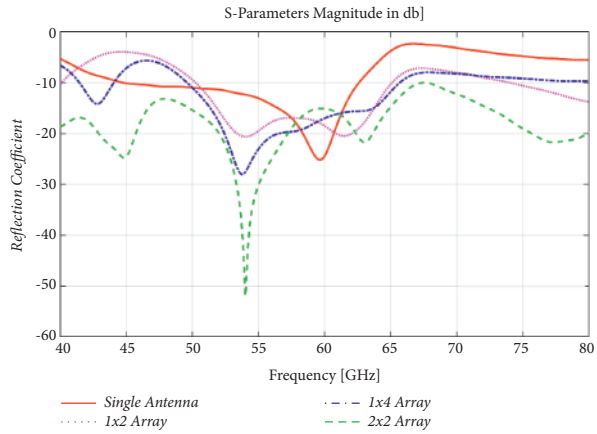

Figure 30: Return loss comparison for different arrangements.

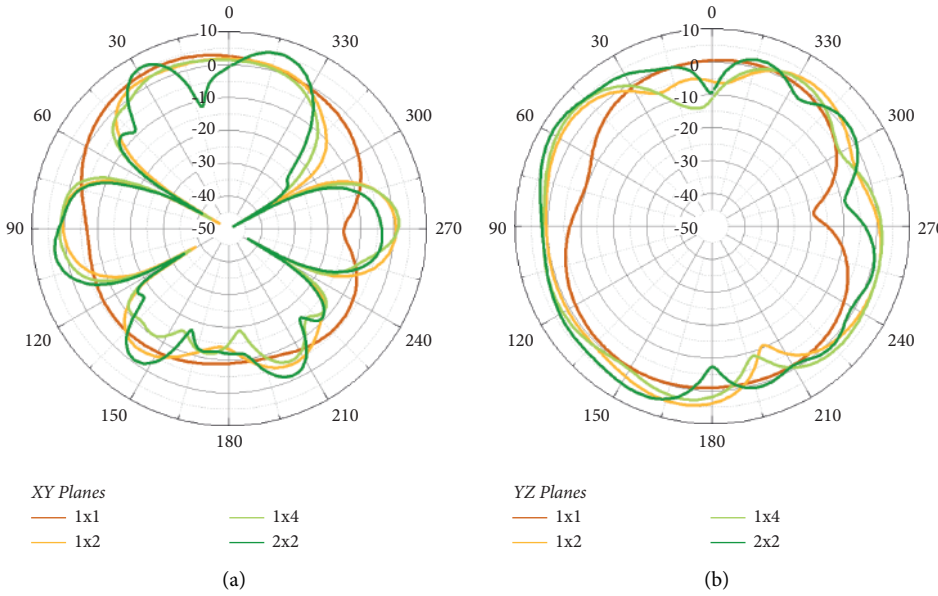

(a) (b)

Figure 31: Return loss comparison for different arrangements on (a) XY plane and (b) YZ plane.

Table 3: Array comparison.

	Single element	1 × 2 array	1 × 4 array	2 × 2 array
Bandwidth	17.8 GHz	15 GHz	16.081 GHz	>27.43 GHz
Gain (dB)	4.01	5.01	5.37	6.65
Radiation efficiency	99.98%	66.16%	66.84%	80.39%
Total efficiency	99.62%	65.22%	65.50%	77.90%
VSWR	1.1283	1.2702	1.3295	1.4273

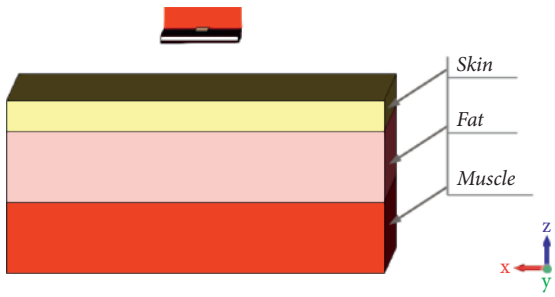

Figure 32: 3D Human body model.

other and the free space parameters. In Figure 34, how the antennas were placed at different distances is shown.

5.1. On-Body Test for Single Antenna (1x1 Design). The solo antenna (1 × 1) was placed at 4 different distances: 2 mm, 4 mm, 6 mm, and 8 mm apart from the created human body model, and simulated the results one by one. The on-body test setup is shown in Figure 35.

All the distances provided similar outcomes in the return loss comparison. In the graph displayed in Figure 36, for the different distances, return losses increased as the distance decreased. The lowest return loss value was found for the 8 mm distance, which was -27.937 dB, while the highest was -18.81 dB for 2 mm. Due to the presence of the human body,

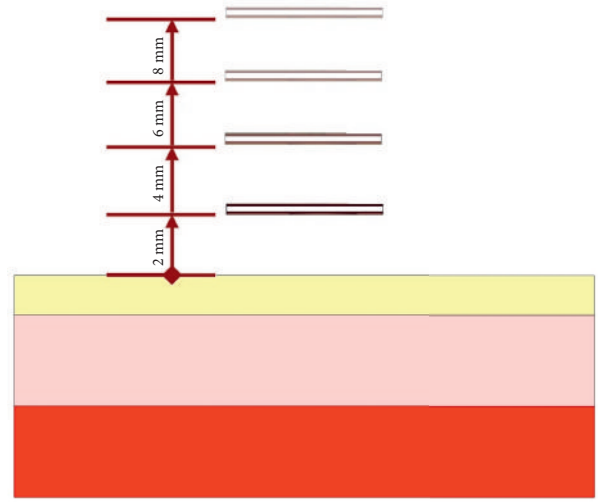

Figure 33: Different distances for on-body simulations.

there is a slight frequency shift noticed when the antenna is placed at different distances from the human body model.

In Figure 37, voltage standing wave ratios for different distances are compared. The changes in the voltage standing wave ratio are similarly relatable to the s11 curve, which was shown in Figure 36. Just like in the return loss comparison plot, the best value was recorded at 8 mm, which was 1.08.

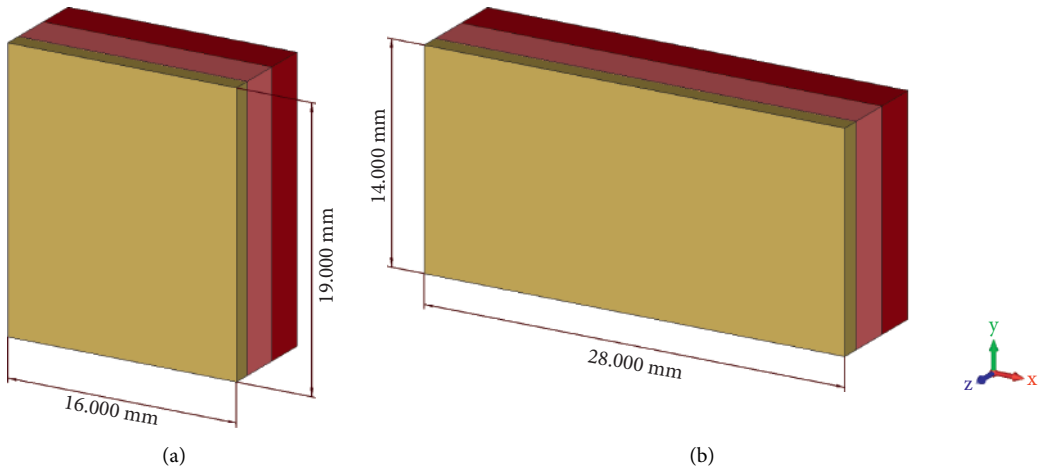

Figure 34: Human body model dimensions (a) for all arrays except 1×4 array and (b) for 1×4 array.

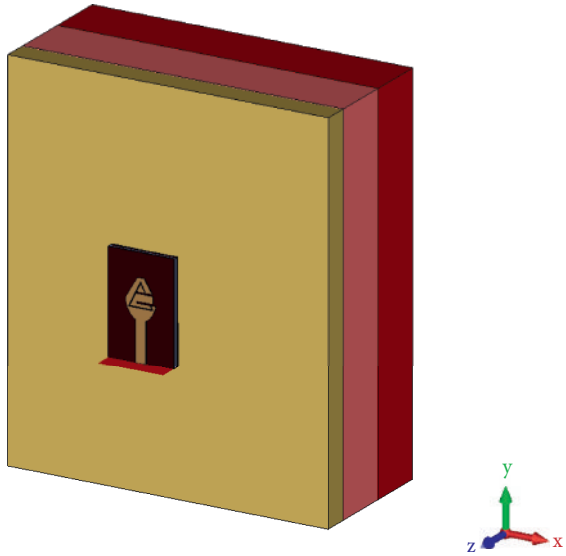

Figure 35: On-Body simulation setup for a single-element antenna.

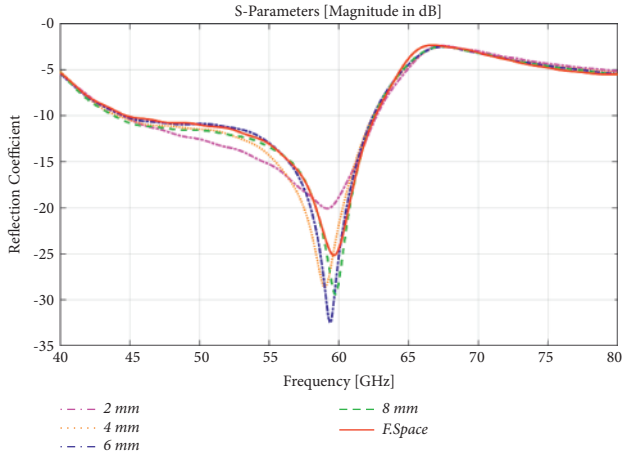

Figure 36: Return loss comparison of the single-element antenna for different distances.

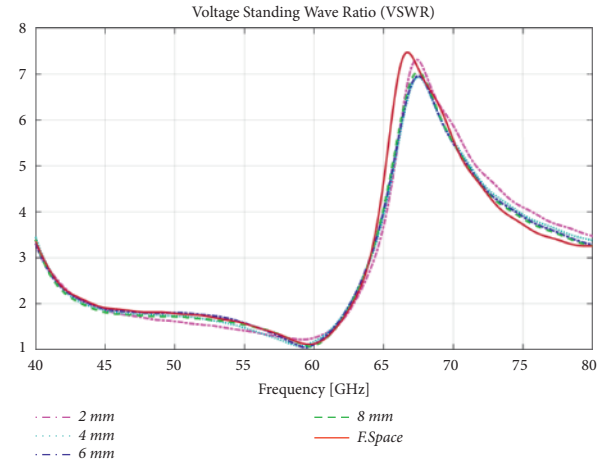

Figure 37: VSWR of the single-element antenna for different distances.

A comparison of the radiation patterns of the solo element antenna for different distances is presented in Figure 38. Except for some gain value fluctuations, there is no discernible change in the patterns found on the XY plane (Figure 37(a)). On the YZ plane, changes are visible in the patterns for the presence of the human body compared to the free space pattern.

In Table 4, other parameters were compared. There were no significant changes in the bandwidth for the presence of the human body or varying its distances. For the rest of the parameters, the results degrade when the antenna is very close to the human body (2 mm) and improve gradually when the distance is increased.

5.2. On-Body Test for 1×2 Array Antenna. The 1×2 antenna array was placed at the selected distances of 2 mm, 4 mm, 6 mm, and 8 mm apart from the 3D human body model. After that, all the results were simulated again for various distances and compared. The on-body test setup for the 1×2 antenna array is shown in Figure 39.

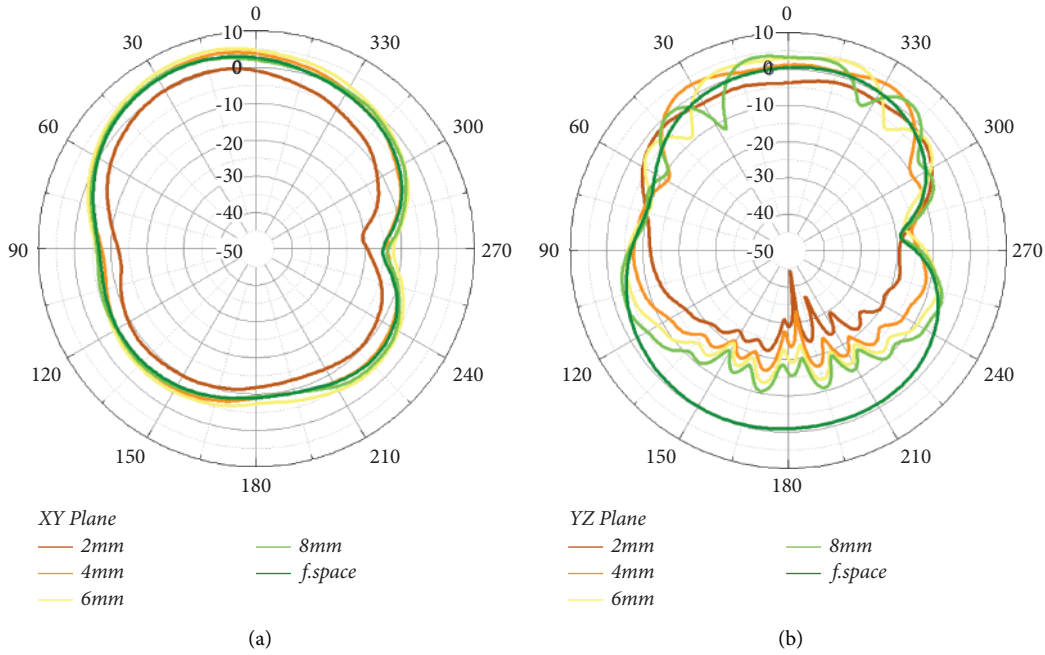

(a) (b)

Figure 38: Radiation patterns of the single-element antenna for different distances (a) on XY plane and (b) on YZ plane.

Table 4: On-body comparison of single-element array for different distances.

Parameters	Free space	On-body 2 mm	On-body 4 mm	On-body 6 mm	On-body 8 mm
Bandwidth (GHz)	17.8	18.24	18.461	17.961	18.722
Return loss (dB) 60 GHz	−24.399	−18.807	−21.771	−25.175	−27.937
Gain (dBi)	4.01	8.41	6.878	6.333	6.48
Radiation efficiency (%)	99.98	75.68	81.74	83.55	85.41
Total efficiency (%)	99.62	74.68	81.19	83.29	85.28
VSWR	1.1283	1.2592	1.1777	1.1168	1.0836

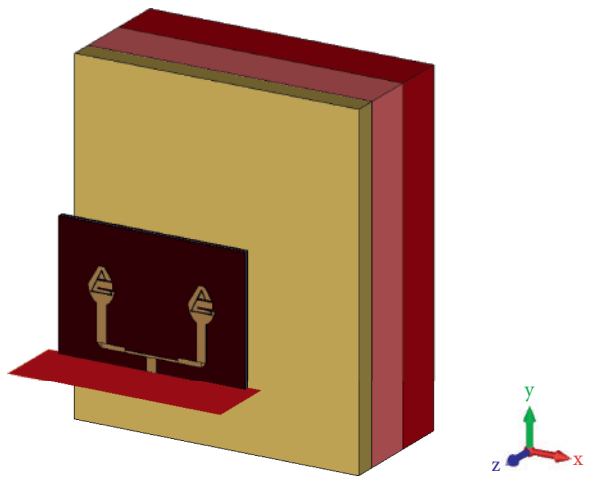

Figure 39: On-Body simulation setup for 1 × 2 antenna array.

In Figure 40, the return losses were compared for the different distances. No significant changes are visible in terms of RL values or bandwidths compared to the free space and on-body results. The minimum return loss value was recorded at -14.32 for an 8 mm distance.

In the VSWR curve shown in Figure 41, the results are very close to unity. All the values fluctuated between 1.38 and 1.48, while the free space value was 1.27. In the distance-based comparisons, the best result was found for 4 mm, which was 1.38.

The results of the radiation pattern comparison on the XY and YZ planes shown in Figure 42 appear to be very stable, even when the array antenna is placed very close to the human body on both planes, with the exception of some minor gain value shifts.

In Table 5, as in previous simulations, there are no major changes in the bandwidth and return loss values for the distance varied body results. The gain and the radiation efficiencies fall a bit for the array antenna when it is placed 2 mm away from the human body model. As the distance increases, these parameters improve gradually, which is quite expected.

5.3. On-Body Test for 1 × 4 Array Antenna. The designed 1 × 4 array antenna was positioned at the preselected four different distances from the 3D human body model. Then, all the results were simulated again for various distances and compared. The on-body simulation setup for the 1 × 4 antenna array is given in Figure 43.

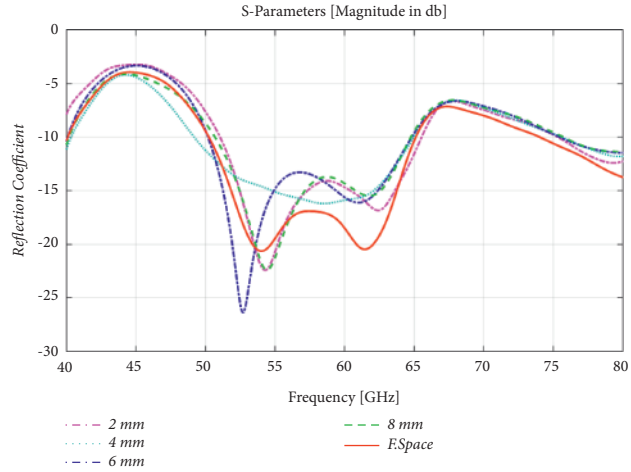

Figure 40: Return loss comparison of the 1×2 array antenna for different distances.

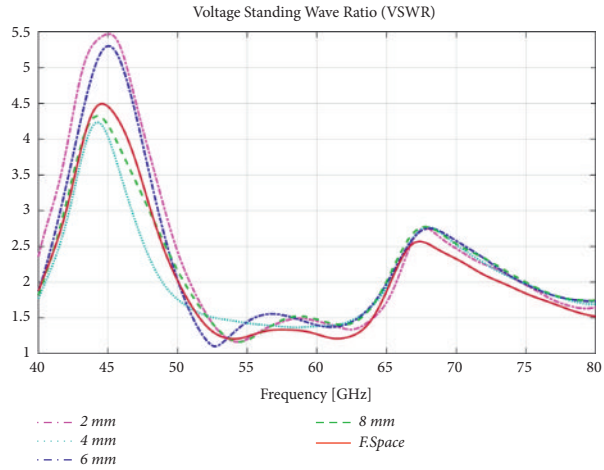

Figure 41: VSWR of the1x2 array antenna for different distances.

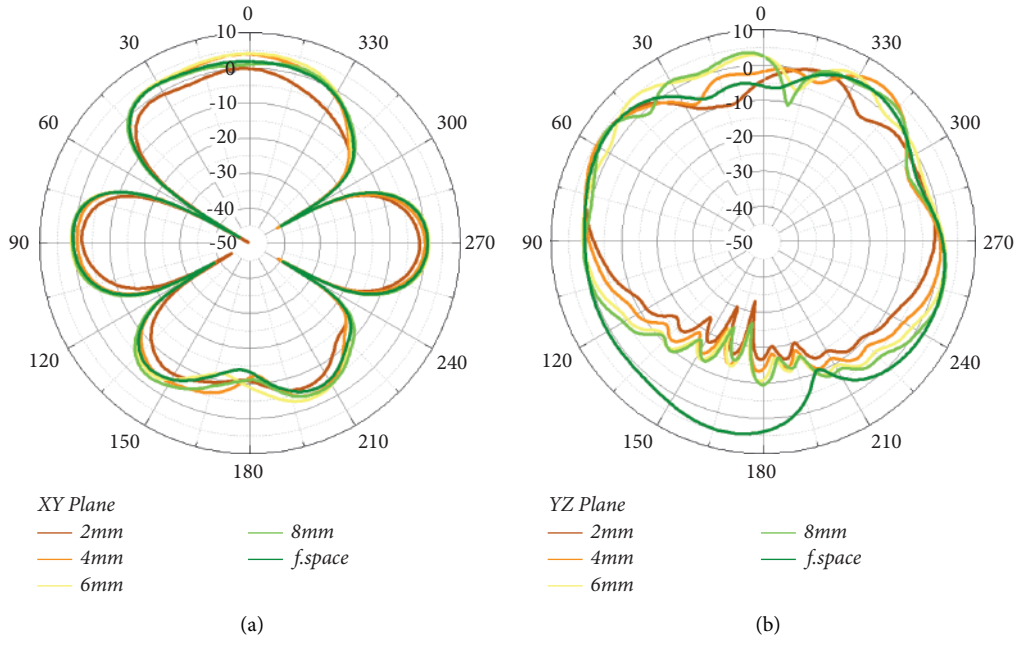

(a) (b)

Figure 42: Radiation patterns of the1x2 array antenna for different distances (a) on XY plane and (b) on YZ plane.

Table 5: On-body comparison of the 1 × 2 array antenna for different distances.

Parameters	Free space	On-body 2 mm	On-body 4 mm	On-body 6 mm	On-body 8 mm
Bandwidth (GHz)	15 GHz	14.527	15.853	14.748	14.078
Return loss (dB) 60 GHz	−18.486885	−14.683668	−15.873721	−15.59942	−14.319633
Gain (dBi)	5.01 dB	6.87	5.303	5.06	4.84
Radiation efficiency (%)	66.16%	43.16	49.10	52.44	55.99
Total efficiency (%)	65.22%	41.69	47.83	50.99	53.92
VSWR	1.2702	1.4523	1.3833	1.398	1.4762

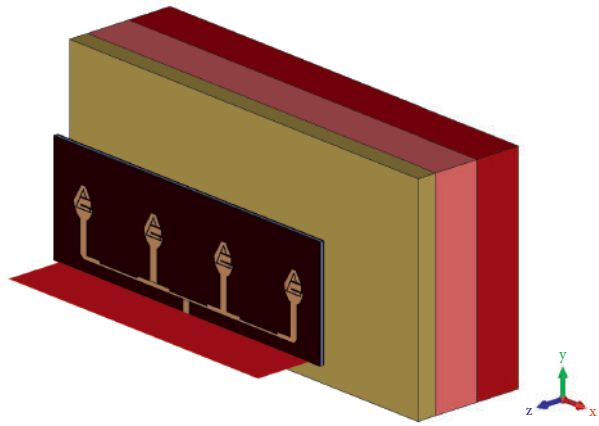

Figure 43: On-Body simulation setup for 1 × 4 antenna array.

The return losses were compared for the different distances in Figure 44. As with earlier results, no significant changes are visible in terms of RL value or bandwidth compared to the free space and on-body results. The minimum return loss value was found for the 8 mm distance, which was -27.937 dB, while the minimum was -18.81 dB for 2 mm.

A slight shift in the resonant frequencies is visible. In the VSWR curve shown in Figure 45, results were oscillating around 1.5. 2D radiation patterns were compared on the XY and YZ planes presented in Figure 46. In both planes, results were very consistent in both the free space and on-body conditions. Distances affected the gain values slightly, but the patterns were very similar.

Table 6 is presented where the gain and the efficiency act like the previously calculated simulation results; values become satisfactory when the distance is greater than 2 mm.

In Table 6, the antenna parameters except the gain for 2 mm distance were a bit degraded, but for other distances, all the other parameters like return losses, gains, or efficiencies improved gradually as the antenna to body gap increased.

5.4. On-Body Test for 2 × 2 Array Antenna. The 2 × 2 arrangement of the array antenna was placed similarly at four different distances (2 mm, 4 mm, 6 mm, and 8 mm) and resimulated the results. Comparisons are given below. Figure 47 shows the on-body simulation setup for the 2 × 2 antenna array.

In Figure 48, the 2 × 2 array had a very wide bandwidth while tested in free space, which was also reflected in the on-body simulation, though the bandwidth was slightly reduced. Rather than this, the results remain much more stable for different distances. The minimum return loss was recorded at 4 mm, which was around −14.319 dB.

Figure 49 shows the voltage standing wave ratio plots comparison for the array antenna's placement at different distances. It shows the VSWR values stayed around 1.5 in different scenarios too. Just like the s11 comparison curve displayed in Figure 48, the antenna showed the best results when placed at a distance of 4 mm. The maximum VSWR value was found to be 1.55 when the antenna was placed closest to the human body model.

In the following figure for the 2D radiation patterns (Figure 50), the array exhibited very consistent results across all the scenarios. Figure 50(a) shows the radiation pattern in the XY plane. Radiation patterns in the YZ plane shown in Figure 50(b) were compared, where the main lobe directions were shifted for different distances.

Table 7 presents other parameter comparisons. In terms of gain and radiation efficiency, for the 2 mm distance, only the gain appears to be higher. However, for stable performance with better values, a 4 mm distance seems more appropriate. Overall, the 2 × 2 array antenna performs satisfactorily.

Table 8 shows a comparison of the proposed antenna in this paper with the published articles. From Table 8, it is noted that the antennas presented in [20–22] are good designs with good performance, but they are proposed for the lower frequency band. A single-element antenna

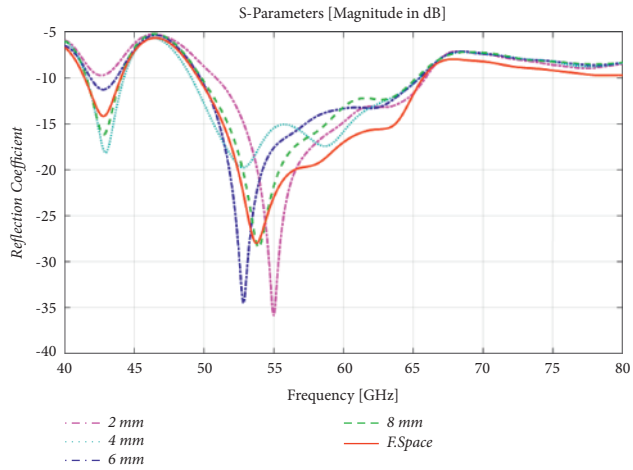

Figure 44: Return loss comparison of the 1×4 array antenna for different distances.

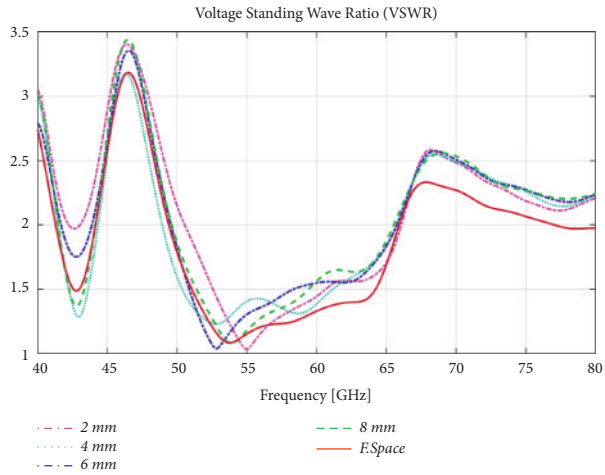

Figure 45: VSWR of 1×4 array antenna for different distances.

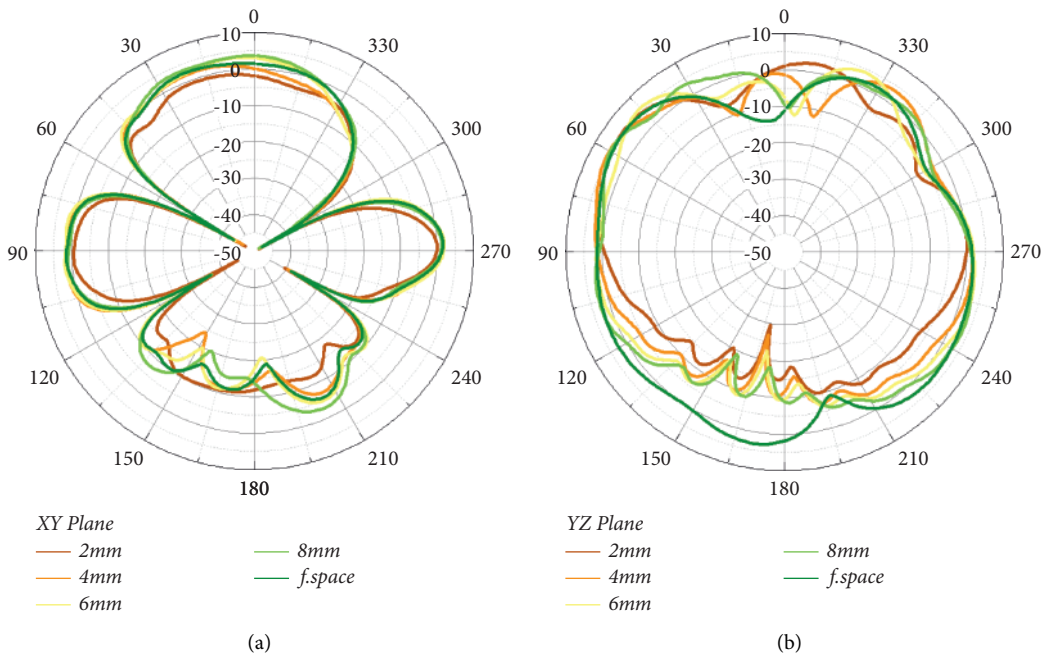

(a) (b)

Figure 46: Radiation patterns of the 1×4 array antenna for different distances (a) on XY plane and (b) on YZ plane.

Table 6: On-body comparison of the 1 × 4 array antenna for different distances.

Parameters	Free space	On-body 2 mm	On-body 4 mm	On-body 6 mm	On-body 8 mm
Bandwidth (GHz)	16.081 GHz	15.153	16.339	15.831	15.41
Return loss (dB) @ 60 GHz	−16.98795	−14.810749	−15.827321	−13.336266	−13.165815
Gain (dBi)	5.37	6.892	5.995	6.537	5.385
Radiation efficiency (%)	66.84%	46.1	48.45	52.35	54.49
Total efficiency (%)	65.50%	44.58	47.19	49.93	51.86
VSWR	1.3295119	1.4442327	1.3857117	1.5489748	1.5629255

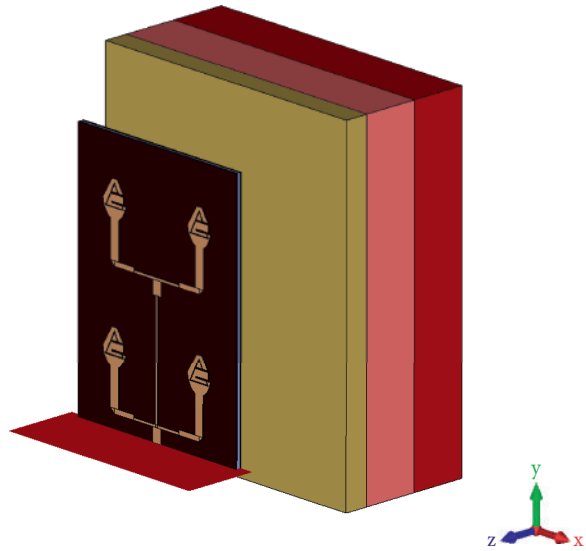

Figure 47: On-body simulation setup for 2 × 2 antenna array.

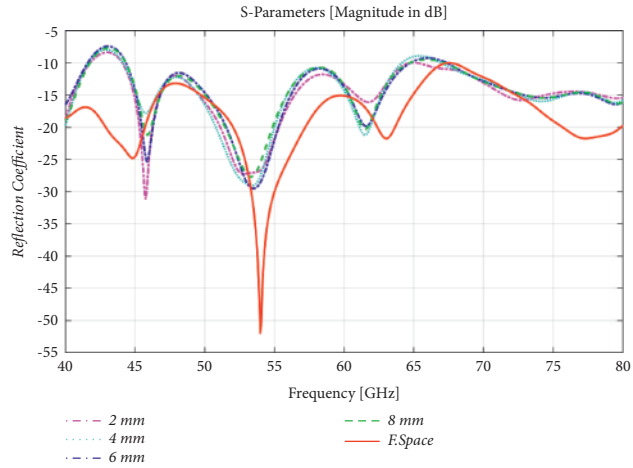

Figure 48: Return loss comparison of the 2 × 2 array antenna for different distances.

working at 60 GHz was proposed for body-centric communication [23]. The antenna is designed on a 100% polyester substrate and it has a 11.632 GHz impedance bandwidth. However, this antenna [23] is not an array antenna, and the overall size of the antenna is bigger compared to the proposed antenna in this study. The antenna proposed in [23] shows lower gain and efficiency compared with the proposed design in this study. In [24], an array antenna is proposed for 60 GHz body-centric communication. The antenna is designed with a cotton substrate [24]. The proposed design in [24] is bigger in size and has low efficiency. The proposed design antenna in this paper has the smallest size with an impedance bandwidth of more than 27.43 GHz. This proposed design also has very good gain and efficiency. The gain and efficiency vary for different array settings. This antenna construction is very new, and it is a small array antenna designed for body-centric communications (BCCs).

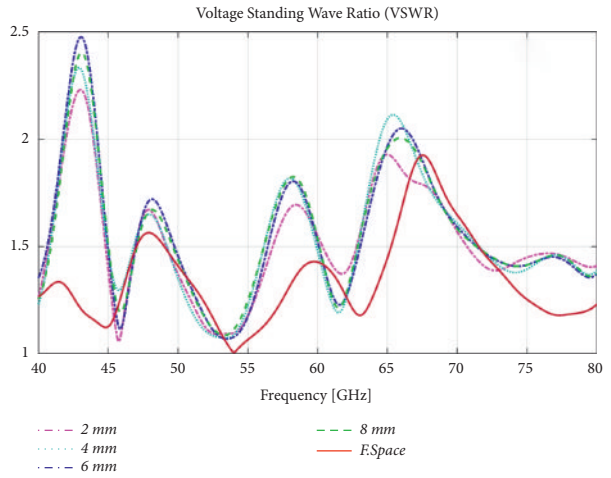

Figure 49: VSWR of 2 × 2 array antenna for different distances.

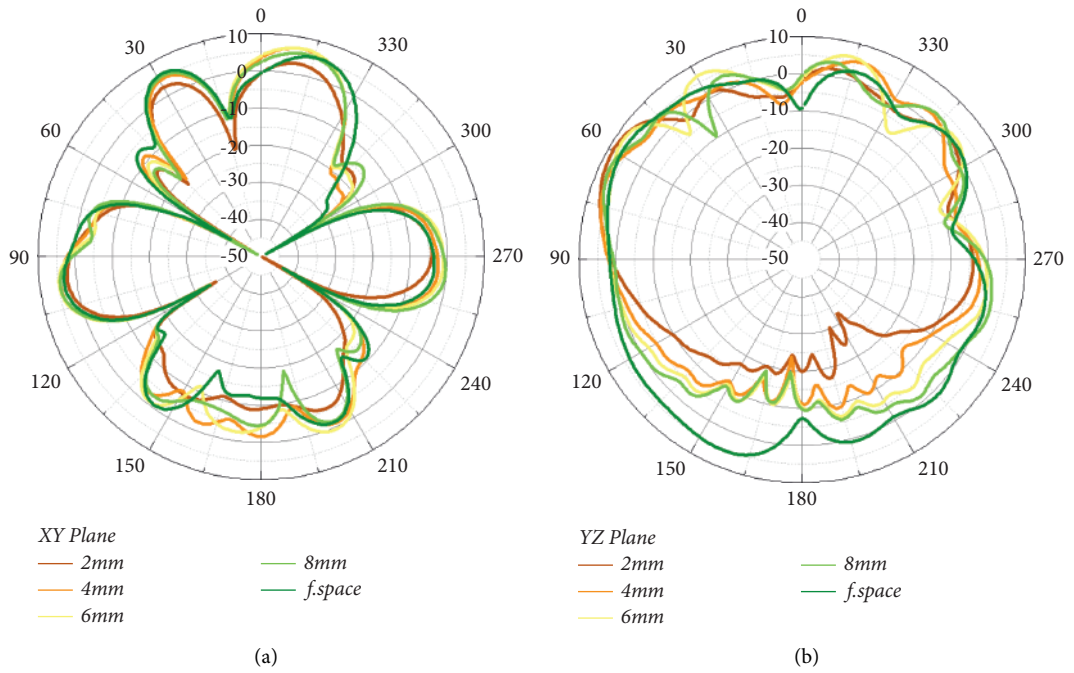

Figure 50: Radiation patterns of the 2 × 2 array antenna for different distances (a) on XY plane and (b) on YZ plane.

Table 7: On-body comparison of the 2 × 2 array antenna for different distances.

Parameters	Free space	On-body 2 mm	On-body 4 mm	On-body 6 mm	On-body 8 mm
Bandwidth (GHz)	>27.43	40	20.121	20.375	20.438
Return loss (dB) 60 GHz	−15.088223	−13.328762	−14.319809	−13.68425	−13.50852
Gain (dBi)	6.65	9.71	8.22	7.87	7.74
Radiation efficiency (%)	80.39%	57.32	62.01	64.15	66.42
Total efficiency (%)	77.90%	54.65	59.72	61.41	63.46
VSWR	1.4272758	1.5495978	1.4762782	1.5218541	1.5353833

Table 8: A comparison of this paper's research with that of other articles.

Antenna	Size length (L) and width (W) mm	Relative permittivity	Substrate	Bandwidth (GHz) at −10 dB	Gain (dBi)	Efficiency (%)	Antenna category
Ref [20]	35.1 × *	2.2	Rogers-RT-duroid-5880	8.63–8.88 9.26–9.66	3.51 4.10	85.2	Duplex filtenna
Ref [21]	30 × 30	2.2	RT/Duroid 5880	8.59–11.43	5.7	*	SIW cavity antenna
Ref [22]	44 × 44	2.2	Rogers RT/ Duroid	9.26–11.02 9.79 to 10.88	5.01 5.30	90	Cavity-backed slot antenna
Ref [23]	12.2 × 12	1.9	100% polyester	11.632	5.96	58.03	Slotted patch
Ref [24]	50 × *	2	Cotton	55–65	8.6	41	Array
This paper single element	5.12 × 3.28	2.2	Rogers RT5880	17.8 GHz	4.01	99.98	Single antenna
This paper 1 × 2 array	7.17 × 10.49	2.2	Rogers RT5880	15 GHz	5.01	66.16	1×2 array
This paper 1 × 4 array	7.17 × 21.38	2.2	Rogers RT5880	16.08 GHz	5.37	66.84	1 × 4 Array
This paper 2 × array	14.33 × 10.48	2.2	Rogers RT5880	More than 27.43 GHz	6.65	80.39	2 × 2 array

*The exact value was not provided.

6. Conclusion

The proposed miniaturized millimeter wave antenna performed satisfactorily with high efficiency near the 60 GHz frequency range (V-band) throughout the different simulations done. The antenna is quite suitable for tiny electronic devices and gadgets because of its smaller dimension and thinner and lighter structure, especially for the wireless body area network (WBAN). For gain and other performance enhancement purposes, several arrays were made with different orders and comparison yielded the most suitable and stable results with the 2 × 2 parallel-fed arrangement. In the human on-body test, the array with 2 × 2 elements showed much better stable performance with sufficient gain, directivity, and efficiency. When the proposed antenna with a 2 × 2 element array is placed on the human body model, it demonstrates 9.71 dBi gain and 57.32% radiation efficiency. In the future, this antenna can be optimized to work in other frequency bands of operation. In addition, a multiple-input and multiple-output (MIMO) algorithm can also be applied to this design [29].

Data Availability

The data used to support the findings of this study are freely available at http://niremf.ifac.cnr.it/tissprop/

Conflicts of Interest

The authors declare that they have no conflicts of interest to report regarding the present study.

Acknowledgments

This research was funded by Princess Nourah bint Abdulrahman University Researchers Supporting Project Number (PNURSP2022R190), Princess Nourah bint Abdulrahman University, Riyadh, Saudi Arabia.

References

[1] IEEE.802.15.Wpantg3c, "Millimeter wave alternative PHY," 2009, http://www.ieee802.org/15/pub/TG3c.html e.

[2] E. C. M. A. Standard, "High rate 60 GHz PHY, MAC & HDMI PAL," 2008, http://www.ecmainternational.org/publications/files/ECMAST/Ecma-387.pdf.

[3] O. Jo, S. H. Chang, C. Y. Kweon, J. Oh, and K. Cheun, "60GHz wireless communication for future wi-fi," *ICT Express*, vol. 1, no. Issue 1, pp. 30–33, 2015.

[4] C. Karnfelt, P. Hallbjorner, H. Zirath, and A. Alping, "High gain active microstrip antenna for 60-GHz WLAN/WPAN applications," *IEEE Transactions on Microwave Theory and Techniques*, vol. 54, no. 6, pp. 2593–2603, 2006.

[5] "V-band on-chip dipole-based antenna," *IEEE Transactions on Antennas and Propagation*, vol. 57, no. 10, pp. 2853–2861, 2009.

[6] Y. P. Zhang, M. Sun, K. M. Chua, L. L. Wai, and L. Duixian Liu, "Antenna-in-package design for wirebond interconnection to highly integrated 60-GHz radios," *IEEE Transactions on Antennas and Propagation*, vol. 57, no. 10, pp. 2842–2852, 2009.

[7] J. Huang, "Practical design of microstrip arrays and reflect arrays," in *Proceedings of the IEEE International Antennas and Propagation Symposium and USNC/CNC/URSI North American Radio Science Meeting*, Columbus, OH, June 2003.

[8] K. Ding, X. Fang, A. Chen, and Y. Wang, "A novel parallel-series feeding network based on three-way power divider for microstrip antenna array," *IEEE Antennas and Wireless Propagation Letters*, vol. 12, pp. 757–760, 2013.

[9] K. Wincza and S. Gruszczynski, "Microstrip antenna arrays fed by a series-parallel slot-coupled feeding network," *IEEE Antennas and Wireless Propagation Letters*, vol. 10, pp. 991–994, 2011.

[10] J. Huang, "A parallel-series-fed microstrip array with high efficiency and low cross-polarization," *Microwave and Optical Technology Letters*, vol. 5, no. 5, pp. 230–233, 1992.

[11] X. M. Zhang, J. L. Huyan, P. C. Gao, H. Wang, and Y. F. Zheng, "Stacked series-fed linear array antenna with

reduced sidelobe," *Electronics Letters*, vol. 50, no. No. 4, pp. 251–253, February. 2014.
[12] T. Metzler, "Microstrip series arrays," *IEEE Transactions on Antennas and Propagation*, vol. 29, no. No. 1, January. 1981.
[13] Y. Chong and D. Wenbin, "Microstrip series fed antenna array for millimeter wave automotive radar applications," *IEEE IMWS*, vol. 1, no. 3, pp. 18–20, 2012.
[14] E. E. Okon and C. W. Turner, "Design of broadband microstrip series array for mm-wave applications," *Electronics Letters*, vol. 38, no. No.18, August. 2002.
[15] P. Mathur, G. Kumar, P. K. Mishra, and Y. K. Verma, "Large gain linear series-fed microstrip antenna arrays at Ka and C bands," in *Proceedings of the 2015 IEEE International Symposium on Antennas and Propagation & USNC/URSI National Radio Science Meeting*, Vancouver, BC, Canada, July 2015.
[16] V. Midasala and P. Siddaiah, "Microstrip patch antenna array design to improve better gains," *Procedia Computer Science*, vol. 85, pp. 401–409, 2016.
[17] Y.-J. Kim, Y.-B. Kim, and H. L. Lee, "mmWave high gain planar H-shaped shorted ring antenna array," *Sensors*, vol. 20, no. 18, p. 5168, 2020.
[18] M. Weiss, "Microstrip antennas for millimeter waves," *IEEE Transactions on Antennas and Propagation*, vol. 29, no. 1, pp. 171–174, 1981.
[19] H. Vettikalladi, W. T. Sethi, and M. A. Alkanhal, "High gain and high efficient stacked antenna array with integrated horn for 60 GHz communication systems," *International Journal of Antennas and Propagation*, vol. 2014, pp. 1–8, Article ID 418056, 2014.
[20] A. Kumar and A. A. Althuwayb, "SIW resonator-based duplex filtenna," *IEEE Antennas and Wireless Propagation Letters*, vol. 20, no. 12, pp. 2544–2548, December. 2021.
[21] A. Kumar and S. Raghavan, "Broadband dual-circularly polarised SIW cavity antenna using a stacked structure," *Electronics Letters*, vol. 53, no. 17, pp. 1171-1172, 2017.
[22] A. Kumar, "Wideband circular cavity-backed slot antenna with conical radiation patterns," *Microwave and Optical Technology Letters*, vol. 62, no. 6, pp. 2390–2397, 2020.
[23] M. M. Khan, K. Islam, M. N. A. Shovon, M. Masud, M. Baz, and M. A. AlZain, "Various textiles-based comparative analysis of a millimeter wave miniaturized novel antenna design for body-centric communications," *International Journal of Antennas and Propagation*, vol. 2021, Article ID 2360440, 14 pages, 2021.
[24] N. Chahat, M. Zhadobov, L. Le Coq, and R. Sauleau, "Wearable endfire textile antenna for on-body communications at 60 GHz," *IEEE Antennas and Wireless Propagation Letters*, vol. 11, pp. 799–802, 2012.
[25] H. M. A. Rahman, M. M. Khan, M. Baz, M. Masud, and M. A. AlZain, "Novel compact design and investigation of a super wideband millimeter wave antenna for body-centric communications," *International Journal of Antennas and Propagation*, vol. 2021, pp. 1–15, Article ID 8725263, 2021.
[26] B. Yang, Z. Yu, Y. Dong, J. Zhou, and W. Hong, "Compact tapered slot antenna array for 5G millimeter-wave massive MIMO systems," *IEEE Transactions on Antennas and Propagation*, vol. 65, no. 12, pp. 6721–6727, December. 2017.
[27] T. Wu, T. S. Rappaport, and C. M. Collins, "The human body and millimeter-wave wireless communication systems: interactions and implications," in *Proceedings of the 2015 IEEE International Conference on Communications (ICC)*, London, UK, June. 2015.
[28] IFAC, "Dielectric properties of body tissues in the frequency range of 10 Hz to 100 GHz," 2022, http://niremf.ifac.cnr.it/tissprop/.
[29] M. Khan, Q. Abbasi, and R. Ashique, "Comprehensive design and propagation study of a compact dual band Antenna for healthcare applications," *Journal of Sensor and Actuator Networks*, vol. 4, no. 2, pp. 50–66, 2015.